

Addressing Barriers to Efficient Renewable Integration

Milestone Report 2

Lead Organisation: University of New South Wales (UNSW)

Project Partners: AEMO, ElectraNet, TasNetworks

Project Commencement Date: 02 July 2018

Project Completion Date: 02 July 2021

Authors: Nelson Fabian Avila, Leonardo Callegaro, Awais Ahmad, Georgios Konstantinou, Jenny Riesz, John Fletcher, Iain MacGill

Contact Name: John Fletcher

Title: Professor, School of Electrical Engineering and Telecommunication

Email: john.fletcher@unsw.edu.au

Date: 15 July 2019

Project Information: <https://arena.gov.au/projects/addressing-barriers-efficient-renewable-integration/>

Inverter Bench Testing Results: <http://pvinverters.ee.unsw.edu.au>

This activity received funding from *Australian Renewable Energy Agency (ARENA)* as part of ARENA's *Emerging Renewables Programme*. The views expressed herein are not necessarily the views of the Australian Government, and the Australian Government does not accept responsibility for any information or advice contained herein.

EXECUTIVE SUMMARY

This technical report presents the details and findings for the project "Addressing barriers to efficient integration of renewables", for the period 05 Jan 2019 to 15 Jul 2019. The specific topics discussed in this report include:

- **Task 1:** Bench testing of 17 commonly used PV inverters in Australia. Five of the selected PV inverters comply with AS 4777.2:2005 and twelve comply with AS 4777.2:2015. The basis of the testing procedure is the application of various voltage and frequency disturbances, the most important being summarized below:
 - response to rapid (100 ms) voltage sags
 - response to phase-angle-jumps (PAJs)
 - response to high rate of change of frequency (RoCoF) with frequency boundary within the limits of AS 4777.2:2005 ($45 \text{ Hz} < g < 55 \text{ Hz}$) and AS 4777.2:2015 ($47 \text{ Hz} < f < 52 \text{ Hz}$).
 - response to frequency deviation within the limits of both versions of AS4777.2
- **Task 2:** The AS4777.2015 standard mandates PV inverters to ride-through short-duration voltage sags, but our results in **D.1.1** indicate otherwise. At present, there is no testing procedure that accredits PV inverters to short-duration voltage sags. Therefore, based on a comparison between the Australian standard and other international standards, such as the one in Germany and the USA, the need of a testing procedure to improve the accreditation of PV inverters to short-duration voltage sags is highlighted. The final objective is to enhance the accreditation process to guarantee that the majority of PV inverters in Australia comply what is mandated in the standard.
- **Task 3:** Development of the WECC Composite Load Model (WECC-CMLD) using a hybrid component-based and measurement-based approach. The component-based approach aggregates the distribution of loads according to standard load classes and the load components of each class to derive the parameters of the aggregate composite load model. On the other hand, the measurement-based approach uses high-sampling-frequency measurements collected at different substations in Australia to derive the most influential parameters of the model (the load composition and the under-voltage protection parameters). The first release of a computational tool to estimate the values of these parameters was developed. The ultimate goal is to minimize the error between the WECC-CMLD output and the collected measurements using state-of-the-art nonlinear optimization solvers. We refer the reader to Section 2 and Section 3 for a thorough description of composite load model and the developed parameter calibration approach.

Contents

1 BENCH TESTING OF PV INVERTERS	7
1.1 Inverter Response to Short-Duration Voltage Sag	7
1.2 Inverter Response to Phase-Angle Jumps	12
1.3 Inverter Response to RoCoF	20
1.4 Response to Frequency Deviations	23
1.5 Outlook on International Standards	26
1.5.1 Short Duration Voltage Sag	26
1.5.2 Phase angle jump	31
1.5.3 Rate of Change of Frequency	32
1.6 Inverters Tested and Power Percentage in the NEM	32
1.7 Conclusions	34
2 THE COMPOSITE LOAD MODEL	35
2.1 WECC-CMLD Description	35
2.2 WECC-CMLD Equations and Parameters	36
2.2.1 Distribution Transformer and Feeder	36
2.2.2 Three-phase Induction Motors (Motor A, B and C)	37
2.2.3 Single-Phase Induction Motor (Motor D)	40
2.2.4 Electronic Loads	42
2.2.5 Static Loads	43
2.3 Final WECC-CMLD States, Variables and Parameters	44
3 WECC-CMLD PARAMETER DERIVATION	45
3.1 Component-based approach	45
3.2 Measurement-based approach	45
3.3 Parameter Estimation Solution	47
3.3.1 Solution algorithm	47
3.3.2 Estimation I:	47
3.3.3 Estimation II	49
3.3.4 Estimation III	51
3.3.5 Additional Experiments	53
3.4 Future Work	56
3.4.1 WECC-CMLD Parameter Estimation	56
3.4.2 Incorporation of DER Dynamics	56
4 CONCLUSIONS	57

List of Figures

1	Schematic of the experimental setup	7
2	Short duration voltage sag test profile	8
3	Example of ride through behaviour (image for Inv. 5 complying with [4])	10
4	Example of power curtailment behaviour (image for Inv. 2 complying with [4])	10
5	Example of curtailment to zero (image for Inv. 4 complying with [4])	11
6	Example of disconnection behaviour (image for Inv. 15 complying with [3])	11
7	Example of phase angle jumps experienced by the grid voltage on a 500 kV line due to a fault [8].	12
8	$\mp 30^\circ$ phase angle variation profile imposed on the inverter ac voltage v_g	12
9	Example of 15° phase jump ride through behaviour (image for Inv. 1 complying with [4]).	15
10	Zoom in of a 15° phase jump showing the ride through behavior of Inv. 1 complying with [4].	15
11	Example of disconnection caused by 30° phase jump (image for Inv. 1 complying with [4]).	16
12	Zoom in of a 30° phase jump showing the disconnection of Inv. 1 complying with [4].	16
13	Example of power curtailment caused by 30° phase jump (image for Inv. 2 complying with [4]).	17
14	Zoom in of a 30° phase jump causing the power curtailment of Inv. 2 complying with [4].	17
15	Example of power curtailment to 0 W caused by 15° phase jump (image for Inv. 10 complying with [4]).	18
16	Zoom in of a 15° phase jump causing power curtailment to zero of Inv. 10 complying with [4].	18
17	Ride through of 90° phase angle jump applied to Inv. 17, complying with [4].	19
18	Zoom in of a 90° phase angle jump showing the ride through behavior of Inv. 17, complying with [4].	19
19	Inverter output power vs. frequency droop characteristic (for inverters without battery storage) [4].	20
20	RoCoF profiles used to test the PV inverters.	21
21	Inverter 5, complying with [4], disconnecting after a 1 Hz/s RoCoF.	23
22	Inverter 4, complying with [4], riding through a 1 Hz/s RoCoF.	23
23	Frequency step test applied to AS 4777.2:2015 compliant inverters.	24
24	Response of Inv. 1 to step increase in frequency from 50 Hz to 51.95 Hz.	25
25	Response of Inv. 5 to step increase in frequency from 50 Hz to 51.95 Hz.	25
26	Response of Inv. 13 to step increase in frequency from 50 Hz to 51.95 Hz (note that at the 20 s time-mark the output power is only decreased slightly).	26
27	Undervoltage ride through capability requirement o DER [5].	27
28	Fault Ride-Through (FRT) limit curve for the voltage curve at the generator terminals for a type 2 power generation unit and for storage units [10, p. 37].	28
29	DER response to abnormal voltages and voltage ride-through requirements for DER of abnormal operating performance Category III [7, Figure H.9 on p. 134].	31
30	Diagram of the WECC Composite Load Model (WECC-CMLD).	35
31	Block diagrams of Motor A,B and C in the WECC-CMLD [15].	38
32	Block diagram of single-phase induction motor (Motor D) [15]	40
33	Developed measurement-based load model tool.	46
34	Feeder X event on October 21 2018 at 14:38.	47
35	Estimation I: Active and reactive power outputs	48
36	Estimation II: Active and reactive power outputs.	49

37	Estimation III: Active and reactive power outputs.	52
38	Event 1: Feeder Y, January 4 2018 at 20:27:39	54
39	Event 2: Feeder Y, May 1, 2018 at 18:27:38	54
40	Event 3: Feeder Y, June 19 2017 at 17:25:38	55
41	Event 4: Feeder Y, July 31, 2018 at 22:51:24	55

List of Tables

1	Passive anti-islanding set-point values, from [4]	8
2	Summary of inverter behaviors due to short duration voltage sag	8
3	Cumulative power in GW of PV systems with size up to 9.5 kW installed to date in Australia [19]	9
4	Power from the inverter tested so far, obtained by multiplying the number of units installed by the power rating of each unit	9
5	Cumulative power of inverters tested not riding-through the short duration voltage sag test	9
6	Power loss due to disconnection or curtailment caused by fast voltage sag, under the hypothesis that all inverters in the NEM behaves like the inverters tested so far	9
7	Phase-angle-jump tests for 2005 inverters	13
8	Phase-angle-jump tests for 2015 inverters	13
9	Cumulative power of inverters not riding-through phase-angle-jump tests	14
10	Power loss due to disconnection or curtailment caused by phase angle jumps, under the hypothesis that all inverters in the NEM behaves like the inverters tested so far	14
11	Summary of inverter behaviors caused by RoCoF stimuli	21
12	Cumulative power of inverters not riding-through RoCoF	21
13	Power loss due to disconnection caused by RoCoF, under the hypothesis that all inverters in the NEM behaves like the inverters tested so far	21
14	Frequency limits for disconnection of the AS4777.3:2005 inverters tested	26
15	Values of voltage and time for the graph of Fig. 27 [5].	28
16	IEEE Std 1547-2015 voltage ride-through requirements for DER of abnormal operating performance Category III [7].	30
17	Power percentage of each tested PV inverter in the National Energy Market	33
18	Inverters to be tested in the next stage of the project	33
19	Load fractions obtained by AEMO (summer peak)	45
20	Load fractions obtained by AEMO (winter peak)	45
21	Estimation I: Parameters in each iteration	48
22	Estimation I: Parameters in each iteration and objective function value	48
23	Estimation II: Parameters and objective function	50
24	Estimation II (cont.): Parameters and objective function.	50
25	Estimation III: Solution when extending the upper and lower bounds of the parameters	51
26	Obtained parameters for additional experiments on various events.	53

1 BENCH TESTING OF PV INVERTERS

Power electronic inverters process the energy produced by PV systems and must ensure continuity of operation under a range of grid disturbances, impacting voltage and frequency at the point of interconnection with the grid. Inverter bench testing has the scope of verifying the inverter response to a variety of events which can occur in the grid. Understanding the behaviour of PV inverters during grid disturbances has multiple benefits, among which are the insights given towards improving existing load models, the information provided to grid operators to manage loads and generation contingencies, and the development of better product standards. The results given by the test benching procedure have highlighted different inverter behaviors in response to specific grid disturbances, the most relevant being described in the coming paragraphs.

The bench testing setup schematic is displayed in Fig. 1. By means of the grid emulator, represented by the ac voltage source v_{emu} , it is possible to change amplitude, frequency and phase parameters of the voltage at the ac connection point of the inverter, v_g . This feature is used to derive the test results presented in the following paragraphs.

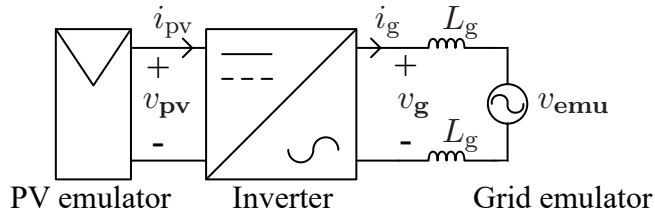


Figure 1: Schematic of the experimental setup

1.1 Inverter Response to Short-Duration Voltage Sag

PV inverters are tested in response to short-duration (100 ms) sags of the ac grid voltage. According to [4], if the terminal voltage of the inverter falls and remains below the under-voltage threshold of 180 V (RMS) for more than 1 s, known as trip delay time, the PV inverter must disconnect from the ac grid within one additional second. In other words, from the time where the voltage falls below 180 V, assuming that the voltage does not recover, the PV inverter must cease operation within 2 s. For voltage sags whose duration is shorter than the trip delay time, the PV inverter is required to remain in continuous operation. Furthermore, during the trip delay time the PV inverter is allowed to continue, reduce or stop the delivery of output power and, if the voltage returns above the limits within the trip delay time, the inverter may resume normal operation. The table below, from [4], reports the voltage and frequency thresholds, as well as the trip delay time and the maximum disconnection time set-points. The standard [4] does not specify a test procedure to verify the inverter ability to withstand voltage sags whose duration is shorter than the trip delay time. The appendix of [4] only specifies a test procedure to check the voltage limits, trip delay and maximum disconnection time, applying an undervoltage causing the disconnection of the inverter. This lack of direction is the cause of a variety of outcomes when PV inverters are subjected to short duration ac voltage sags.

During the bench testing, the test profile in Fig. 2 was applied on each PV inverter. The stimulus consists of one 100 ms 0.78 p.u. voltage sag, bringing the grid voltage (v_g in Fig. 1) from 230 to 50 V. In other words, the voltage sag is removed before the trip delay time of 1 s.

These are the main behaviours observed in response to the stimulus of Fig. 2:

- inverter rides-through the voltage sag, returning to the operational regime existing prior to the event, once the voltage sag has elapsed

Table 1: Passive anti-islanding set-point values, from [4]

Protective function	Protective function limit	Trip delay time	Maximum disconnection time
Undervoltage (V<)	180 V	1 s	2 s
Overvoltage 1 (V>)	260 V	1 s	2 s
Overvoltage 2 (V>>)	265 V	—	0.2 s
Under-frequency (F<)	47 Hz (Australia) 45 Hz (New Zealand)	1 s	2 s
Over-frequency (F>)	52 Hz	—	0.2 s

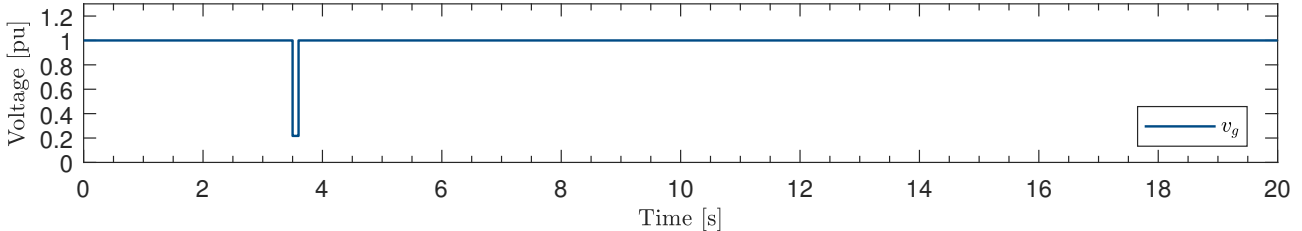


Figure 2: Short duration voltage sag test profile.

Table 2: Summary of inverter behaviors due to short duration voltage sag

	2005 inverters			2015 inverters		
	Inv.	Brand	Total	Inv.	Brand	Total
Nºof inv. riding through	14	E	1	1, 6, 7/3, 13/5/17	A/C/E/G	7
Nºof inv. disconnecting	8/15	A/F	2	11	F	1
Nºof inv. curtailing ($P > 0$)	-	-	-	2/16	B/D	2
Nºof inv. curtailing ($P = 0$)	-	-	-	4, 10, 12	D	3
Nºof inv. with other behavior	6/9	A/B	2	-	-	-
Total Nºof inv. tested			5			13

- inverter reduces (curtails) its power output and resumes operation at the pre-fault power level after several minutes
- inverter curtails its active power to zero, but remains connected and resumes operation at the pre-fault power level after more than 5 minutes
- inverter disconnects from the ac grid and resumes operation at the pre-fault power level after more than 5 minutes

The responses of inverters tested complying with AS 4777.3:2005 and of the ones complying with AS 4777.2:2015 are summarised in Table 2.

Table 3 reports the cumulative power of PV installations sized up to 9.5 kW in each state and in the NEM. These data were sourced from the Australian Photovoltaic Institute (APVI) website [19]. The power and percentage of inverters in each state that does not ride-through the short duration voltage sag is reported in Table 5. In this table, the power values were calculated by multiplying the power rating of the inverters tested by number of inverters installed in each state. The latter figure was sourced by interrogating the Clean Energy Regulator database [18]. The percentage values in Table 5 have been calculated dividing the power figure in the same table by the total power given by

Table 3: Cumulative power in GW of PV systems with size up to 9.5 kW installed to date in Australia [19]

	NSW	VIC	QLD	SA	WA	TAS	NT	NEM
GW	1.5	1.29	2.1	0.79	0.94	0.11	0.05	6.78

Table 4: Power from the inverter tested so far, obtained by multiplying the number of units installed by the power rating of each unit

	NSW	VIC	QLD	SA	WA	TAS	NT	NEM
MW	100	90	306	46	45	9	6	603

Table 5: Cumulative power of inverters tested not riding-through the short duration voltage sag test. The percentage figure is obtained by dividing the power reported in the table by the total DER power in a state or the NEM (considering DER of power up to 9.5 kW)

	NSW	VIC	QLD	SA	WA	TAS	NT	NEM
MW	24	37	43	16	15	2	1	138
%	2	3	2	2.0	2	2	2	2

Table 6: Power loss due to disconnection or curtailment caused by fast voltage sag, under the hypothesis that all inverters in the NEM behaves like the inverters tested so far

	NSW	VIC	QLD	SA	WA	TAS	NT	NEM
MW	361	527	292	278	303	29	9	1549
%	24	41	14	35	32	26	16	23

PV installations with power up to 9.5 kW present in each state and in the NEM, and summarised in Table 3.

So far the inverters tested in the lab represent about 9.22% of all inverters installed in the NEM (see Table 17). If the remaining portfolio of inverters failed the fast voltage sag test with the same distribution of the 9.22% of inverters tested so far, then Table 6 represents a broader estimate of the power at risk of disconnection or curtailment. Note that the distribution of inverters failing a certain test varies among different states, depending on the inverter brands and number of units installed. For instance, in NSW the power from inverters tested add up to 100 MW (in Table 4), and the power from inverters which fail the fast voltage sag test add up to 24 MW (i.e. 24%, in Table 5). If the estimate is based uniquely upon the results of bench testing, then the percentage of all inverters disconnecting in NSW is projected to be 24% ($= 100 \times \frac{24 \text{ MW}}{100 \text{ MW}}$) of the total DER power installed in NSW (1.5 GW from Table 3) from PV systems sized up to 9.5 kW, i.e. $24\% \times 1.5 \text{ GW} = 361 \text{ MW}$, as reported in Table 6 (noting that numbers have been rounded to the nearest integers).

Typical waveforms for the behaviors noted in Table 2 are displayed in the following graphs. The calculated RMS ac voltage and current, \tilde{V}_{ga} and \tilde{I}_g , are in the top plot, the PV voltage and current, V_{pv} and I_{pv} , are in the middle plot (these are DC values), and the calculated instantaneous active and reactive power, \tilde{P}_g and \tilde{Q}_g (as defined in [6]), are in the bottom plot of each figure.

- Ride-through behavior:

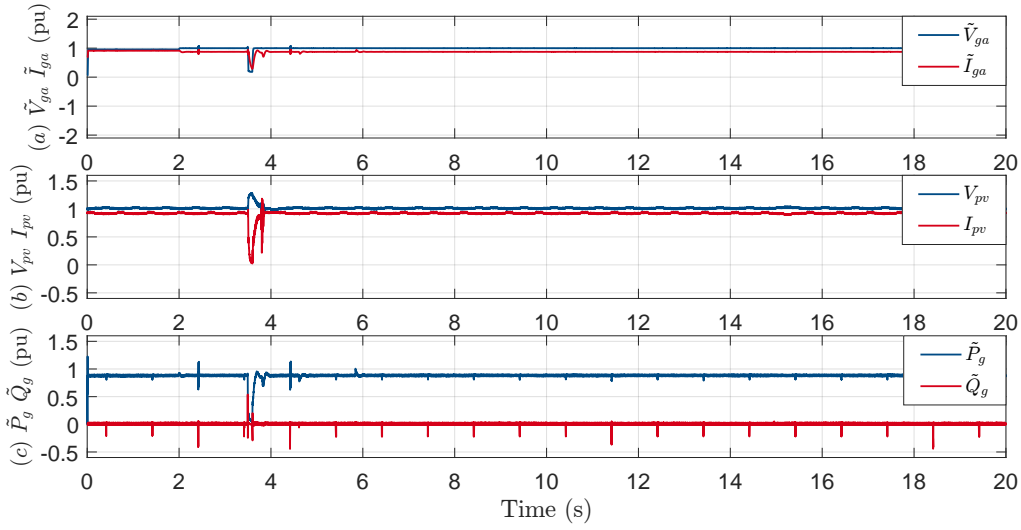


Figure 3: Example of ride through behaviour (image for Inv. 5 complying with [4]). Note that the active power, \tilde{P}_g , quickly resumes the value it had prior to the disturbance after the voltage sag is removed.

- Curtailment:

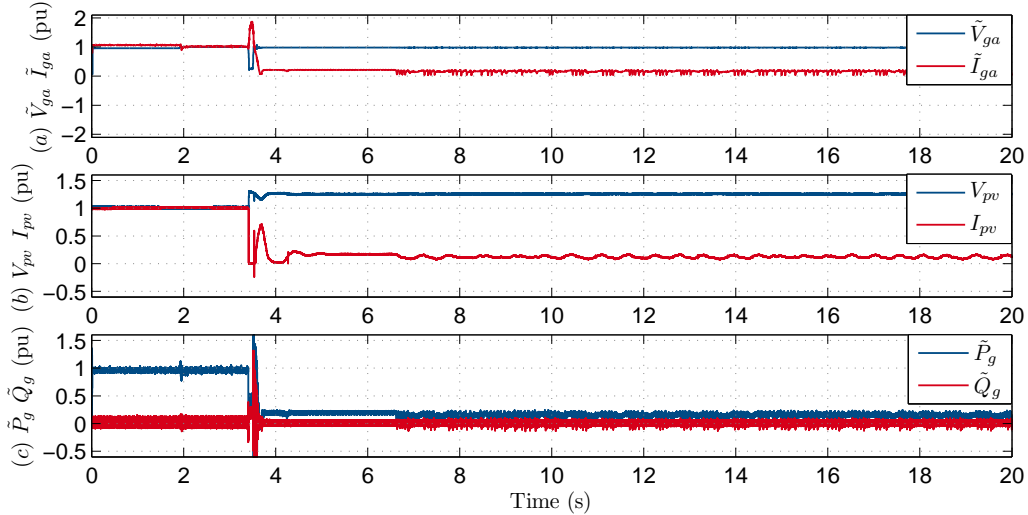


Figure 4: Example of power curtailment behaviour (image for Inv. 2 complying with [4]). Note that the active power, \tilde{P}_g , is reduced significantly after the voltage sag is cleared.

- Inverter curtailing power to zero whilst remaining connected:

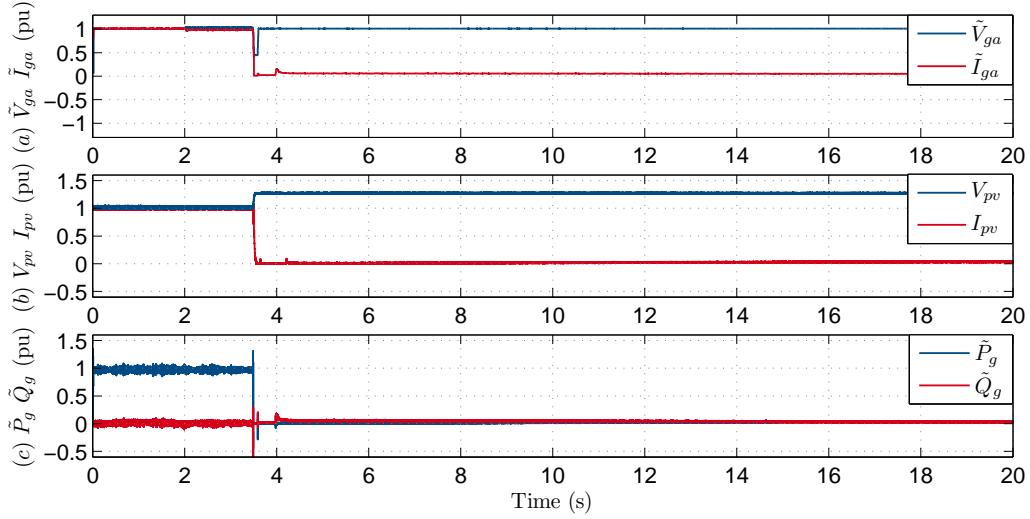


Figure 5: Example of curtailment to zero (image for Inv. 4 complying with [4]). Note that the active power, \tilde{P}_g , after the voltage stimulus is equal to zero. The inverter then takes more than 5 min to resume operation at full power.

- Disconnection:

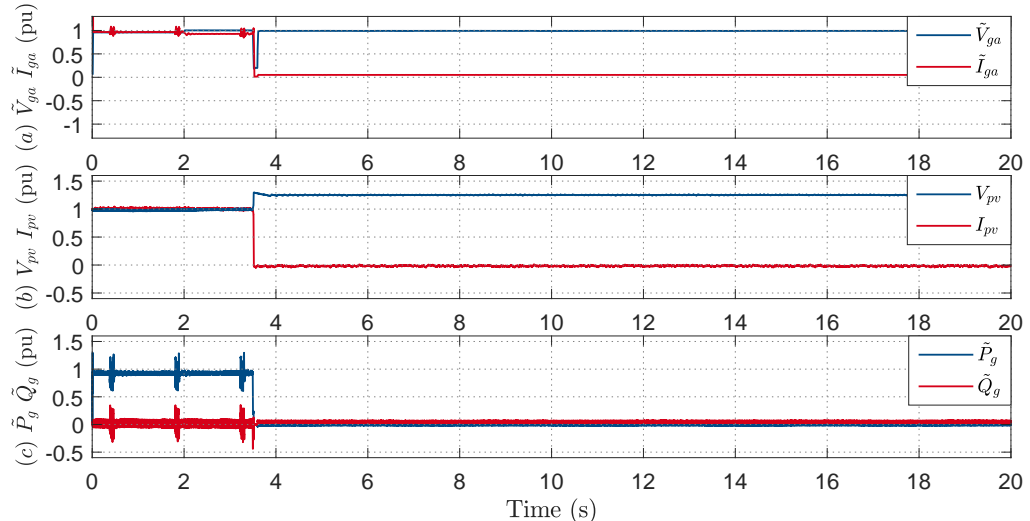


Figure 6: Example of disconnection behaviour (image for Inv. 15 complying with [3]). Note that the active power, \tilde{P}_g , is equal to zero after the voltage sag is cleared. The inverter takes between 1 and 2 min to resume operation at full power.

In conclusion to this section, bench testing has highlighted issues with inverters complying with either of the Australian standards of interest [3] or [4]. The instances where the PV inverter disconnects from the ac grid following a 100 ms voltage sag, taking minutes to resume operation at the pre-disturbance power level, can result in sudden aggregated loss of generation in the power system, which may affect its stable operation.

1.2 Inverter Response to Phase-Angle Jumps

International legislation, and notably the IEEE Standard 1547-2018 [7, p. 58], require DER connected inverters to withstand phase angle jumps occurring in the grid voltage. Fig. 7 displays the voltage measurement on a 500 kV line in southern California (USA) experiencing phase angle jumps caused by a fault (Blue Cut Fire event in 2016, see [8] for details).

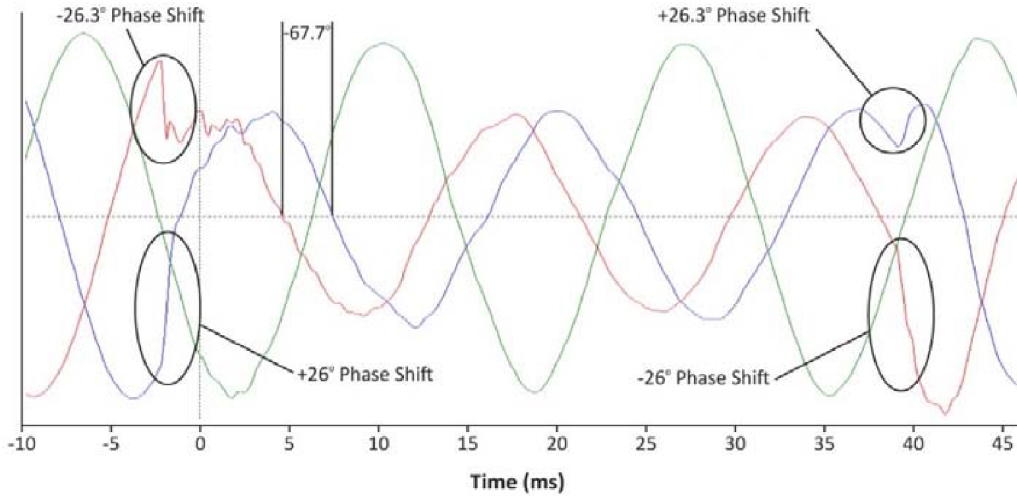


Figure 7: Example of phase angle jumps experienced by the grid voltage on a 500 kV line due to a fault [8].

While it is apparent that phase angle jumps occur as consequence of faults in the transmission network (see [9] for an in-depth explanation), an understanding of the phase jump propagation from the transmission level to the low voltage distribution level, where PV inverters are connected, remains the objective of future work. Nevertheless, bench testing has once again proven valuable to assess an inverter behaviour following phase angle jumps in the grid voltage. Eighteen PV inverters, of which five complying with AS 4777.3:2005 and thirteen complying with AS 4777.2:2015, have been tested against 15° and 30° phase angle jump, with the majority of them also being tested for 45° and 90° phase angle jump.

Table 7 and Table 8 present the outcome of the phase jump tests executed on inverters complying with AS 4777.3:2005 and AS 4777.2:2015, respectively. The test profile applied is a repetition of the one displayed in Fig. 8, showing the modulation of the grid voltage phase angle ($\pm 30^\circ$ in the figure).

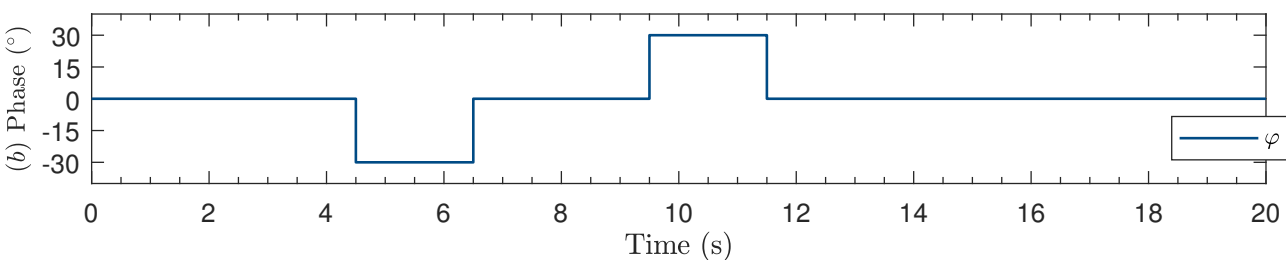


Figure 8: $\pm 30^\circ$ phase angle variation profile imposed on the inverter ac voltage v_g .

Table 7: Phase-angle-jump tests for 2005 inverters

Inv.	Brand	15°	30°	45°	90 °
6	A	✓	✓	✓	✓
8	A	✓	✓	✓	X
9	B	✓	✓	X	X
14	E	✓	✓	✓	X
15	G	✓	X	X	X

Table 8: Phase-angle-jump tests for 2015 inverters

Inv.	Brand	15°	30°	45°	90°
1	A	✓	X	-	-
2	B	✓	curtail	X	X
3, 13	C	✓	✓	✓	✓
4	D	P=0	curtail	P=0	P=0
5	E	✓	✓	✓	✓
6	A	✓	X	X	X
7	A	✓	curtail	P=0	P=0
10	D	P=0	P=0	P=0	P=0
11	F	X	X	-	-
12	D	P=0	P=0	P=0	P=0
13	C	✓	✓	✓	✓
16	D	✓	✓	✓	curtail
17	G	✓	✓	✓	✓

In Table 7 and Table 8, the checkmark “✓” indicates that the inverter rides through the phase angle jump without any significant change of output power, the cross “X” indicates the disconnection of the inverter from the ac grid following the phase angle jump. The sign “P=0” indicates a power reduction to zero, while “curtail” means that the power output was reduced, but remained greater than zero; in such cases the inverter would require more than 5 min to resume operation at the pre-fault power level.

Table 9 presents a summary of inverters which did not ride through the phase angle jump test, for a phase angle jump of 15°, 30°, 45° and 90°. The power value in this table were obtained by multiplying the power rating of the inverters tested, by the number of units installed in the field. The percentage values were obtained by dividing the power values in Table 9 by the figures given in Table 3.

Table 9: Cumulative power of inverters not riding-through phase-angle-jump tests (note: the percentage figure is a ratio between the cumulative power in MW and the total DER power of inverters up to 9.5 kW installed in a state or in the NEM)

Not riding through PAJ		NSW	VIC	QLD	SA	WA	TAS	NT	NEM
15°	MW	5	13	11	3	4	1 5	0	36
	%	0.3	1.0	0.5	0.4	0.4	0.9	0	0.5
30°	MW	20	32	34	11	11	2	1	113
	%	1	3	2	1	1	2	2	2
45°	MW	34	39	54	22	17	3	4	173
	%	2	3	3	3	2	2	8	3
90°	MW	43	50	145	28	23	6	5	299
	%	3	4	7	4	2	6	9	4

Table 10: Power loss due to disconnection or curtailment caused by phase angle jumps, under the hypothesis that all inverters in the NEM behaves like the inverters tested so far

Not riding through PAJ		NSW	VIC	QLD	SA	WA	TAS	NT	NEM
15°	MW	71	188	73	54	78	12	0	410
	%	5	15	3	7	8	11	0	6
30°	MW	307	462	235	195	236	22	8	1266
	%	20	36	11	25	25	20	15	19
45°	MW	515	558	368	371	360	30	42	1947
	%	34	43	18	47	38	27	78	29
90°	MW	639	722	990	483	470	73	43	3366
	%	43	56	47	61	50	65	80	50

As discussed for the fast voltage sag, if all inverters installed in the NEM had the same response to phase angle jump similar to the 9.22% of NEM inverters tested so far, a broader projection on the power disconnecting or curtailment in each state is possible, and is reported in Table 10.

Waveform of typical inverter behavior in response to a phase jump stimulus are displayed in the next pages.

- Phase angle jump ride-through

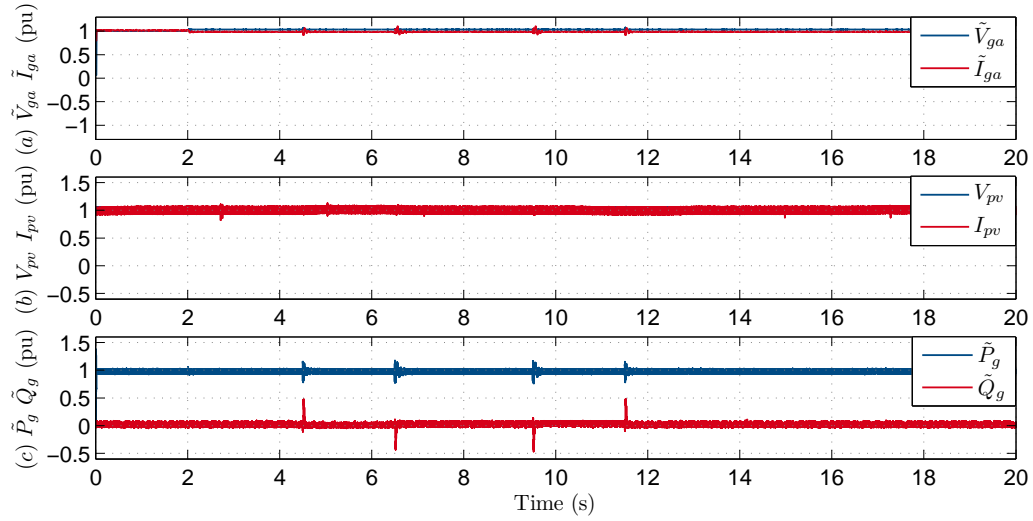


Figure 9: Example of 15° phase jump ride through behaviour (image for Inv. 1 complying with [4]).

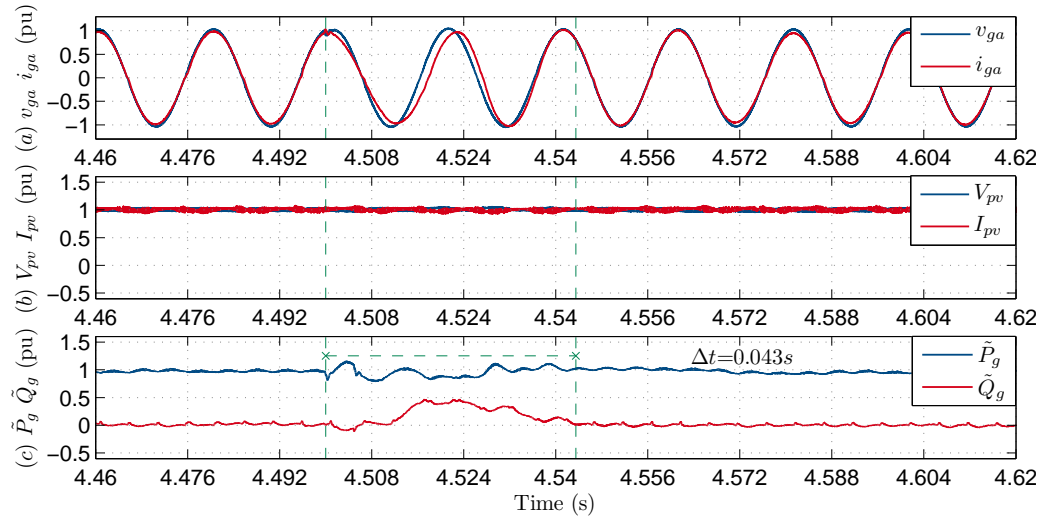


Figure 10: Zoom in of a 15° phase jump showing the ride through behavior of Inv. 1 complying with [4].

- Phase angle jump causing inverter disconnection

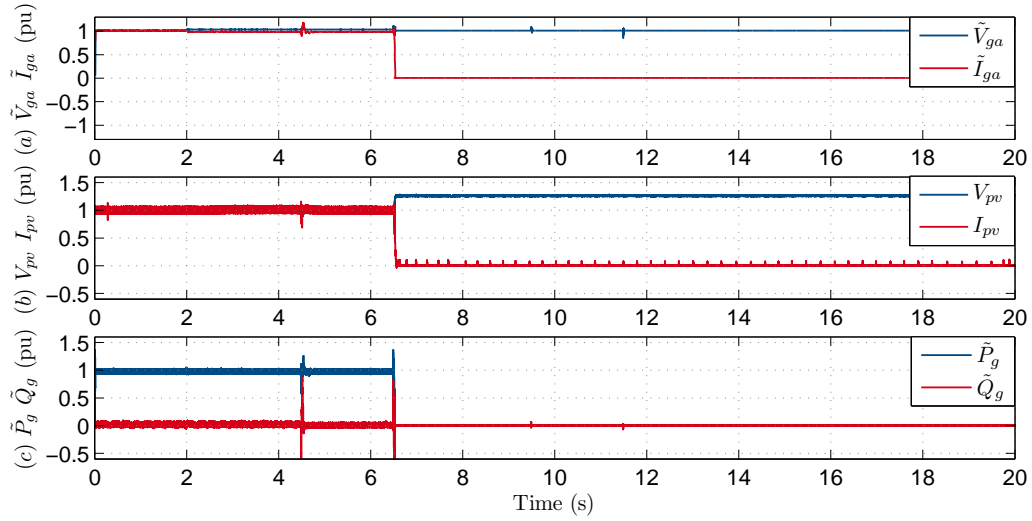


Figure 11: Example of disconnection caused by 30° phase jump (image for Inv. 1 complying with [4]).

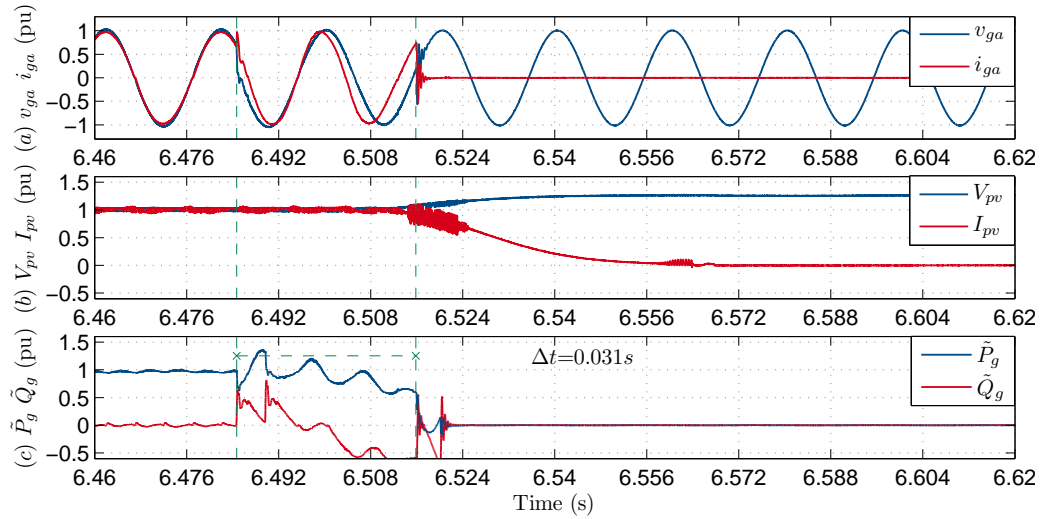


Figure 12: Zoom in of a 30° phase jump showing the disconnection of Inv. 1 complying with [4].

- Phase angle jump causing reduction of output power

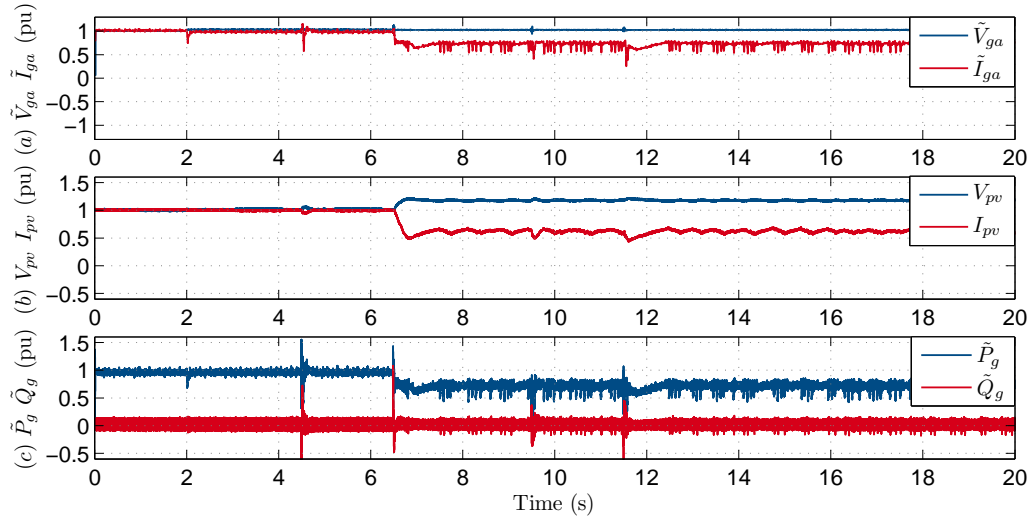


Figure 13: Example of power curtailment caused by 30° phase jump (image for Inv. 2 complying with [4]).

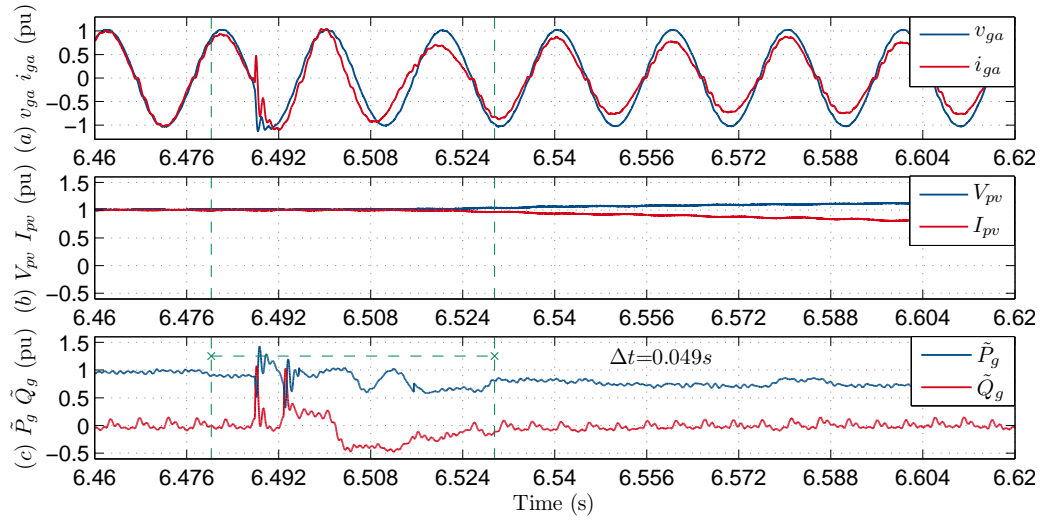


Figure 14: Zoom in of a 30° phase jump causing the power curtailment of Inv. 2 complying with [4].

- Phase angle jump causing output power curtailment to 0 W (this case is equivalent to a disconnection, since the inverter takes more than 5 min to resume operation at the pre-fault power level)

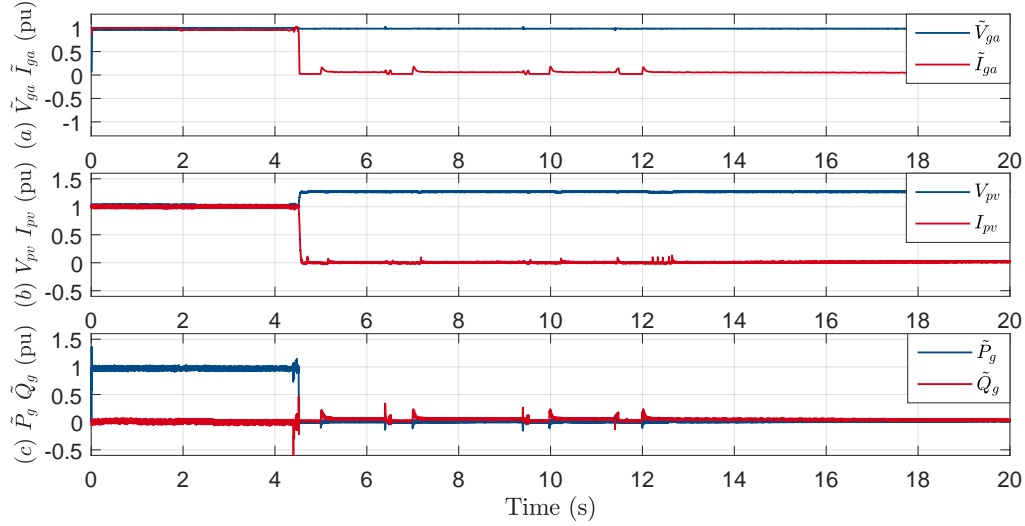


Figure 15: Example of power curtailment to 0 W caused by 15° phase jump (image for Inv. 10 complying with [4]).

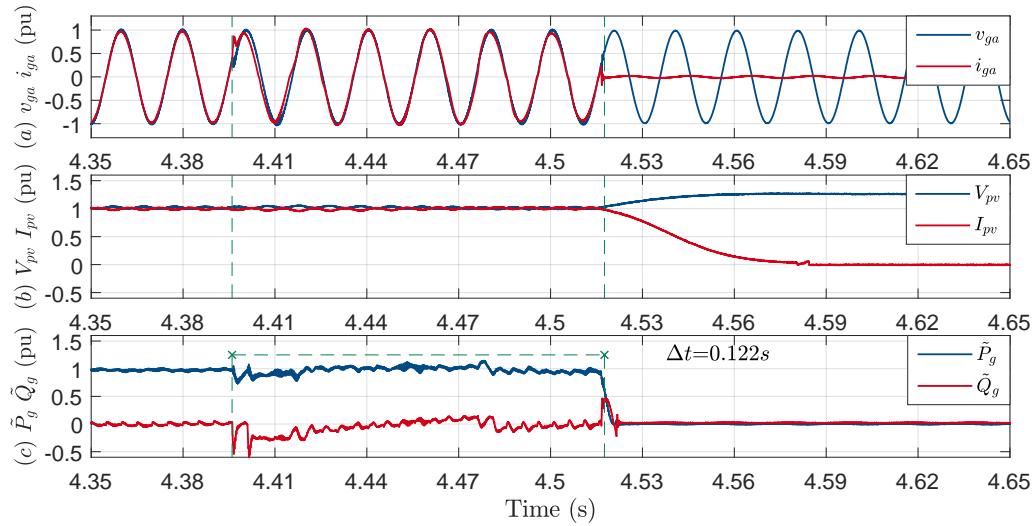


Figure 16: Zoom in of a 15° phase jump causing power curtailment to zero of Inv. 10 complying with [4].

Finally, it is worth reporting the waveforms of a phase angle jump of 90° which is rode through by an inverter, demonstrating that this is achievable.

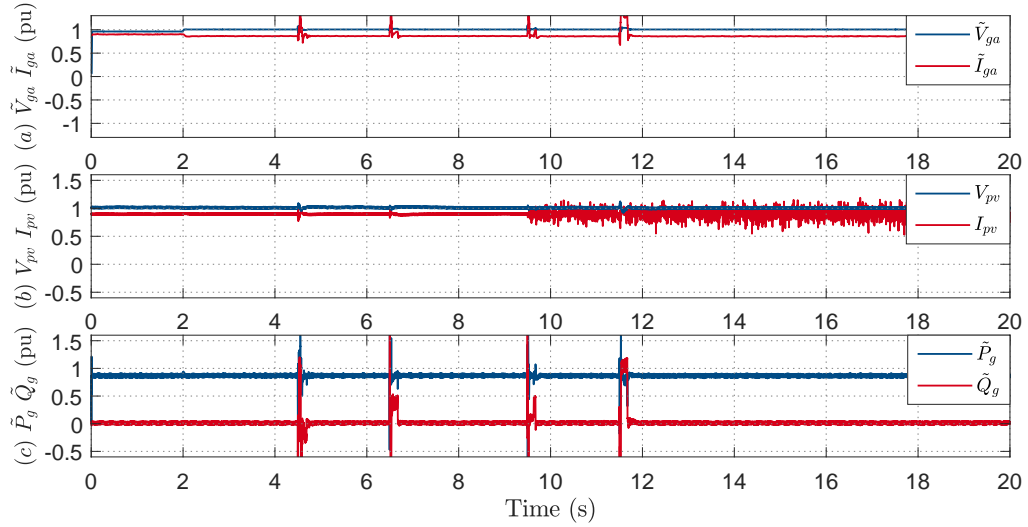


Figure 17: Ride through of 90° phase angle jump applied to Inv. 17, complying with [4].

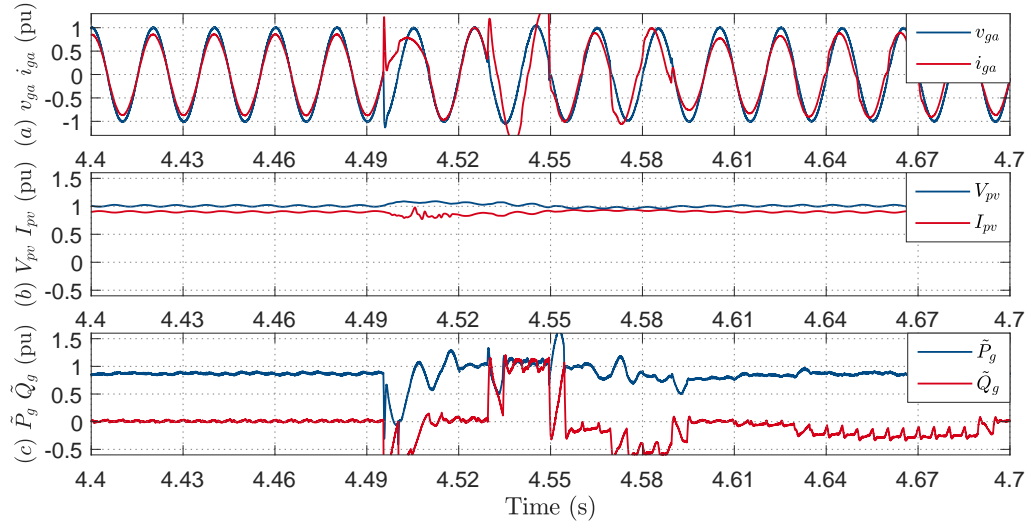


Figure 18: Zoom in of a 90° phase angle jump showing the ride through behavior of Inv. 17, complying with [4].

In summary, the bench testing results obtained by applying phase angle jump stimuli demonstrated very different outcomes depending on the inverter make and models. Of particular concern are the instances where the phase angle jump causes the disconnection of the inverter, and the inverter takes several minutes before resuming operation at the pre-fault power level. The same can be said about the cases when the output power is reduced to zero (although without disconnecting from the grid) following a phase angle jump, and the inverter takes several minutes to reestablish operation at full power.

It is important that future version of the Australian Standard mandate phase angle jump withstand-ing requirements for DER inverters.

1.3 Inverter Response to RoCoF

Unbalance between generation and demand in the BPS may lead to undesired frequency deviations from the nominal value ($\Delta f = f_0 - f$). The grid frequency (f) may not abruptly drift from the nominal value ($f_0 = 50$ Hz), instead, it varies linearly between two different steady-state points. The slope of such ramp is also known as the rate of change of frequency (RoCoF), in Hz/s. The current Australian standard [4] mandates that PV inverters remain connected if $47 \text{ Hz} \leq f \leq 52 \text{ Hz}$, eventually regulating their output power as shown in Fig. 19. Assuming the inverter is delivering the power P_{ref} to the grid, should the grid frequency f increase over 50 Hz, the output power of the inverter, P_{out} , is reduced linearly according to:

$$P_{\text{out}} = P_{\text{ref}} \left[1 - \frac{f - 50.25}{f_{\text{stop}} - 50.25} \right], \quad (1)$$

where $f_{\text{stop}} = 52$ Hz.

In order to evaluate the response of different commercial PV inverters to frequency disturbances in the power grid, frequency excursions with RoCoF of 1 Hz/s, 4 Hz/s and 10 Hz/s were applied in the terminal ac voltage, v_g , according to the profiles depicted in Fig. 20, where $f_{\text{stop}} = 51.95$ Hz.

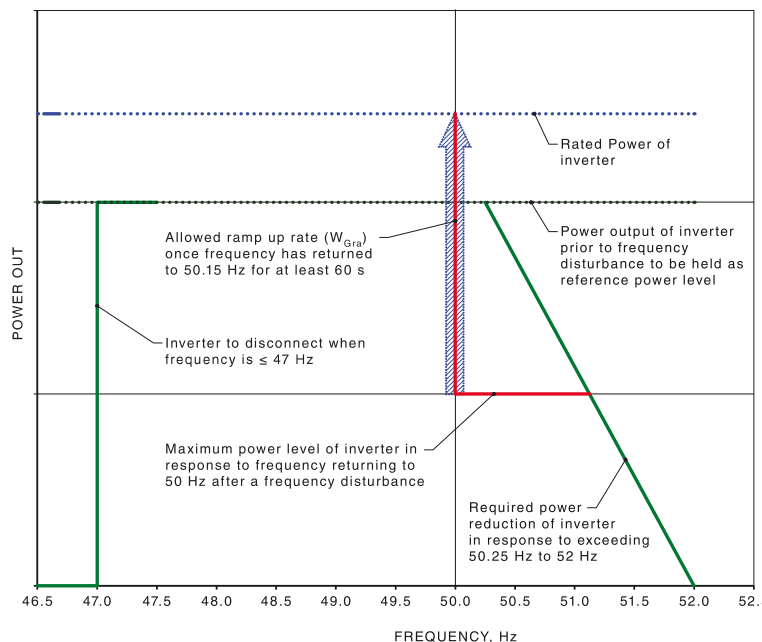


Figure 19: Inverter output power vs. frequency droop characteristic (for inverters without battery storage) [4].

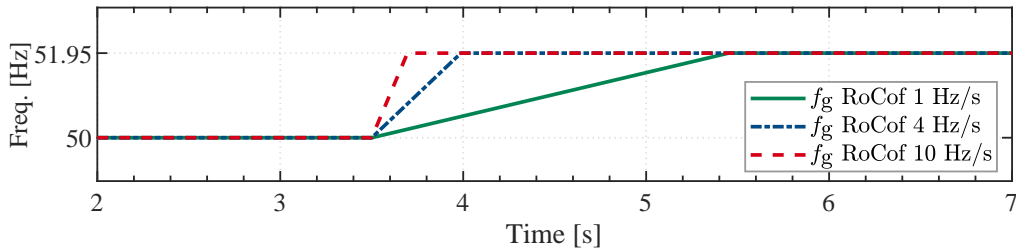


Figure 20: RoCoF profiles used to test the PV inverters.

Table 11: Summary of inverter behaviors caused by RoCoF stimuli

	2005 inverters			2015 inverters		
	Inv.	Brand	Total	Inv.	Brand	Total
Nºof inv. disconnecting @ 10 Hz/s	-	-	-	4	D	1
Nºof inv. disconnecting @ 1, 4, 10 Hz/s	14	E	1	5	E	1
Nºof inv. riding through @ 1, 4, 10 Hz/s	all others		4	all others		11
Total Nºof inv. tested			5			13

Table 12: Cumulative power of inverters not riding-through RoCoF. The percentage figure is a ratio between the power reported in the table and the total DER power in a state or the NEM, for DER up to 9.5 kW

Not riding through 1 Hz/s RoCoF		NSW	VIC	QLD	SA	WA	TAS	NT	NEM
Inv. 5 & Inv. 14	MW %	22 1	21 2	165 8	12 2	9 1	5 5	0 1	234 3

Table 13: Power loss due to disconnection caused by RoCoF, under the hypothesis that all inverters in the NEM behaves like the inverters tested so far

Not riding through 1 Hz/s RoCoF		NSW	VIC	QLD	SA	WA	TAS	NT	NEM
Inv. 5 & Inv. 14	MW %	323 22	301 23	1129 54	207 26	178 19	61 55	4 7	2629 39

Since $f_{stop} < 52$ Hz, it is expected that the PV inverter will remain connected to the grid at the chosen f_{stop} . It is important to mention that the current version of [4] does not specify any requirements against RoCoF. The results from the experiments performed are reported in Table 11, while Table 12 reports the percentage of inverters tested (known in each state) not riding through some or all RoCoF.

Assuming the percentage of inverter tested to be representative of all the inverters installed in the NEM, then a wider projection on the power and percentage of inverter disconnecting is reported in Table 13.

The RoCoF tests highlighted that:

1. the majority of the inverters tested were able to withstand RoCoF up to 10 Hz/s remaining connected to the ac grid
2. three inverters complying with AS 4777.2:2015 disconnected due to RoCoF. Out of these, one of them is an inverter from a relatively new manufacturer, whose market share in Australia is negligible (Inv. 11). Another inverter (Inv. 4) disconnected for a RoCoF of 10 Hz/s and was able

to ride-through 4 Hz/s and 1 Hz/s, and the last inverter disconnected for a RoCoF as low as 1 Hz/s (Inv. 5).

3. one inverter complying with AS 4777.3:2005 (Inv. 14) disconnects for RoCoF as low as 1 Hz/s. This inverter is from the same manufacturer of the last inverter mentioned in point 2 above.

As an example, a disconnection caused by a 1 Hz/s RoCoF, and 1 Hz/s RoCoF ride-through behavior are displayed in Fig. 21 and Fig. 22, respectively. While in the former instance the disconnection is highlighted by an abrupt power drop to zero, in the latter instance the decrease of power occurs smoothly and the inverter is still connected to the ac grid.

- RoCoF causing disconnection

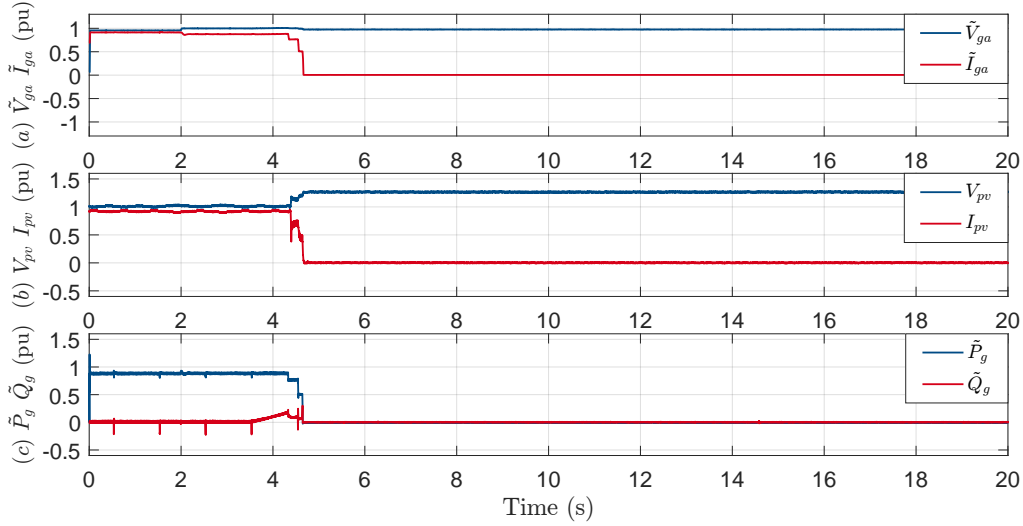


Figure 21: Inverter 5, complying with [4], disconnecting after a 1 Hz/s RoCoF.

- RoCoF being rode-through (and activating the active power vs. frequency response)

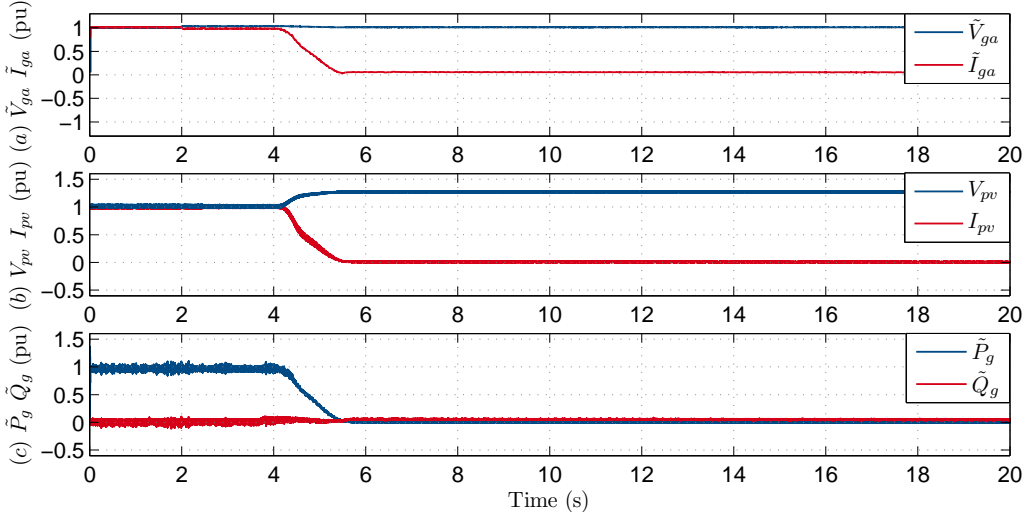


Figure 22: Inverter 4, complying with [4], riding through a 1 Hz/s RoCoF.

In conclusion, while most of the PV inverters tested rode through the RoCoF disturbances without disconnecting from the ac grid, one inverter brand (2005 and 2015 models) shown to be vulnerable and disconnect from the grid for RoCoF as low as 1 Hz/s.

1.4 Response to Frequency Deviations

The Australian standards AS 4777.3:2005 and AS 4777.2:2015 prescribe the frequency boundaries where the inverter must remain connected with the ac grid. The former standard specifies $45 \text{ Hz} < f < 55 \text{ Hz}$, while the frequency limit specified in the latter standard is $47 \text{ Hz} < f < 52 \text{ Hz}$. These

limits are verified in the bench testing process by applying steps in the frequency. As an example a test performed on AS 4777.2:2015 complying inverters is shown in Fig. 23.

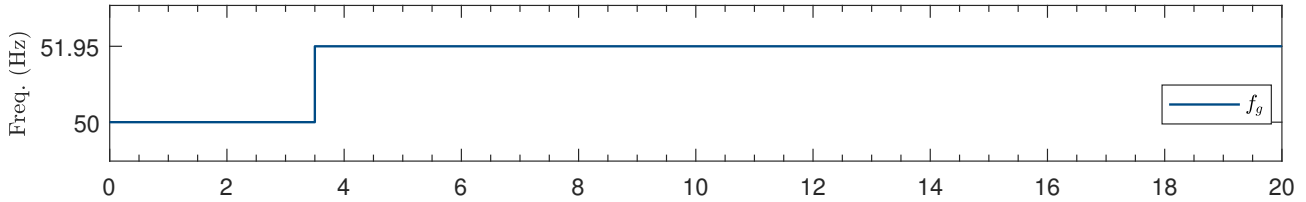


Figure 23: Frequency step test applied to AS 4777.2:2015 compliant inverters.

This test allows to verify two features of AS 4777.2:2015 compliant inverters. First, the inverter must remain connected to the ac grid unless it is tripping due to RoCoF, and second, it is possible to observe the activation of the active power vs. frequency droop response.

Out of thirteen AS 4777.2:2015 compliant inverter tested, only three disconnected following the stimulus displayed in Fig. 23. The disconnection of these inverters can be attributed to their sensitivity to RoCoF, since these were the same inverters which did not withstand RoCoF of 10 Hz/s, and a frequency step can be assumed to be a RoCoF stimulus with $\Delta f / \Delta t \gg 10 \text{ Hz/s}$.

Another important observation from this test emerges from the calculated active power. In fact, stepping the frequency from 50 to 51.95 Hz means that the AS 4777.2:2015 compliant inverter must decrease its active power output according to the power vs. frequency droop curve of Fig. 19. This test allows to verify the different response time of each inverter in reducing the active power output. Typical inverter behaviors are displayed in the following figures (where the frequency is stepped at the 3.5 s time-mark):

- Reduction of active power output occurs quickly, in about 1 s, following the frequency step (desired behavior):

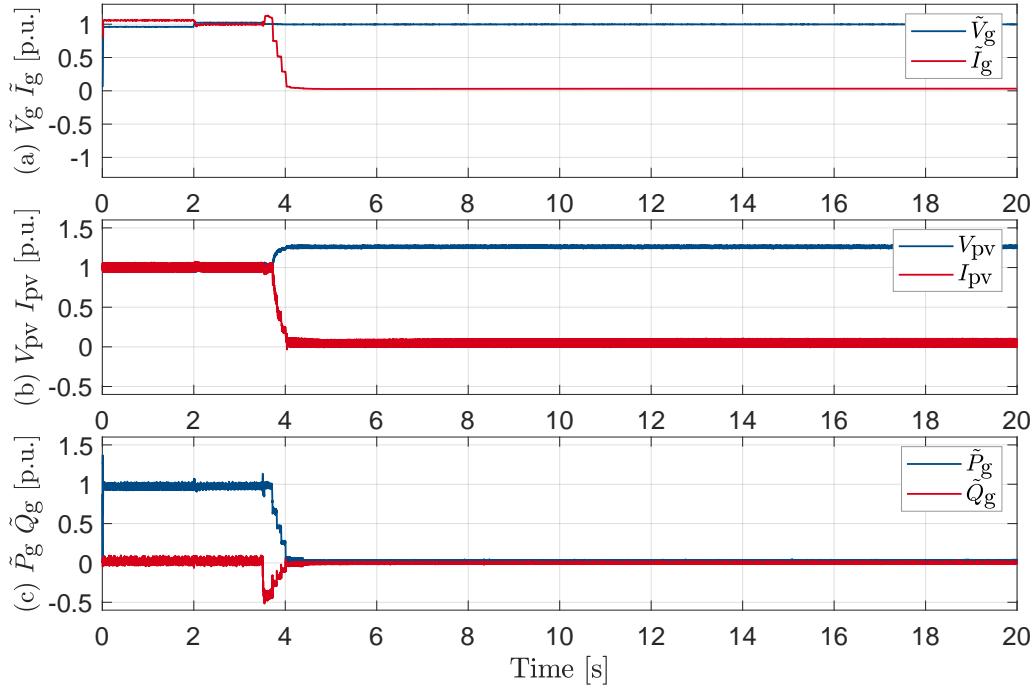


Figure 24: Response of Inv. 1 to step increase in frequency from 50 Hz to 51.95 Hz.

- Reduction of active power output takes 2 to 3 s following the frequency step:

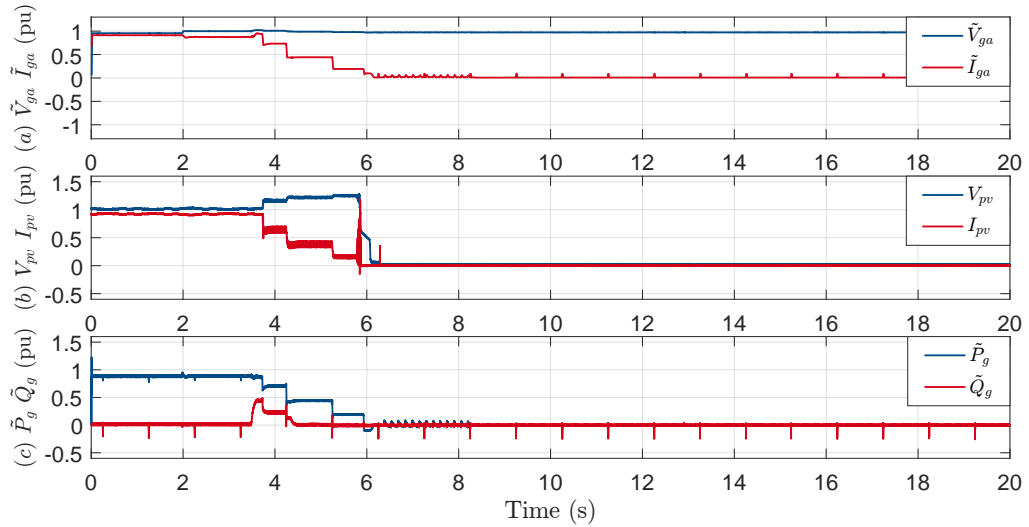


Figure 25: Response of Inv. 5 to step increase in frequency from 50 Hz to 51.95 Hz.

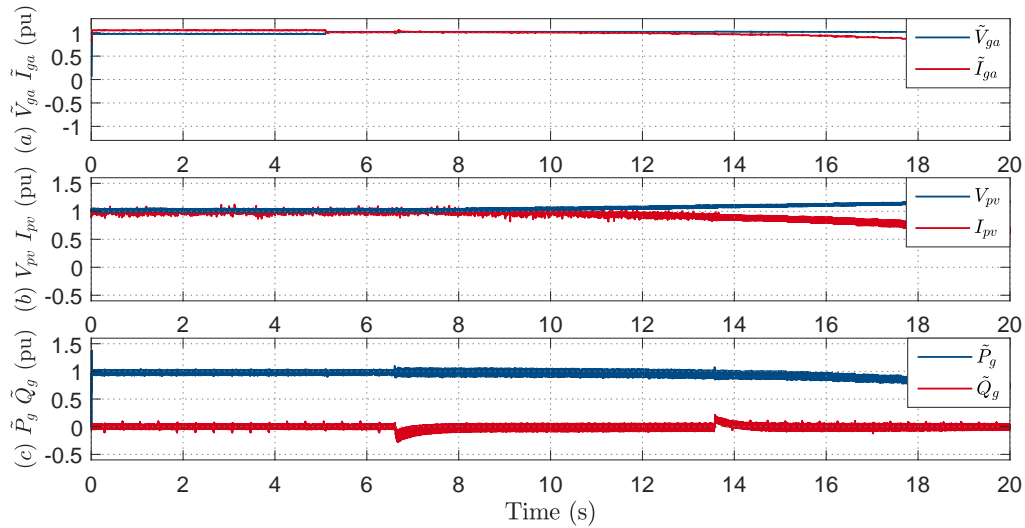


Figure 26: Response of Inv. 13 to step increase in frequency from 50 Hz to 51.95 Hz (note that at the 20 s time-mark the output power is only decreased slightly).

Table 14: Frequency limits for disconnection of the AS4777.3:2005 inverters tested

Inverter	Frequency Limits
6	45 Hz < f < 55 Hz
8	48 Hz < f < 52 Hz
9	49 Hz < f < 51 Hz
14	47 Hz < f < 53 Hz
15	49.5 Hz < f < 50.5 Hz

- Reduction of active power output takes more than 20 s following the frequency step (undesired behaviour):

Inverters complying with AS 4777.2:2015 operate within 47 Hz and 52 Hz. Inverters complying with AS 4777.3:2005, do not have any active power vs. frequency droop response implemented. For these category of inverters, the frequency step test has allowed to verify the variety of frequency disconnection thresholds among different inverter manufacturers. AS 4777.3:2005 in fact states that the limit for disconnection can be any value within 45 and 55 Hz. The frequency disconnection limits derived thanks to the bench testing process are reported in Table 14.

1.5 Outlook on International Standards

The main results from inverter bench testing have been described in the previous sections. Through the bench testing process it was verified that inverters complying with the most recent Australian standards may still be vulnerable to grid disturbances, especially phase angle jumps, short duration voltage sags and RoCoF. This evidence has prompted to enquire whether international standards take these grid disturbances into account and mandate that inverter should withstand them.

1.5.1 Short Duration Voltage Sag

AS 4777.2:2015 briefly deals with short duration voltage sags, only when specifying the inverter behaviour if an undervoltage condition is cleared within the *trip delay time* of 1 s. The standard

"requires the inverter to remain in continuous, uninterrupted operation for voltage variations with a duration shorter than the trip delay time specified in [Table 1]". Moreover, a note in AS 4777.2:2015 states:

When voltage falls below the undervoltage limit of [Table 1] it is permissible to continue, reduce or stop the inverter output during the trip time delay and if voltage returns above the limit during the trip time delay period [the inverter] may resume normal operation.

AS 4777.2:2015 then refers to its Section G to verify the undervoltage (and overvoltage) trip settings. However, Section G does not include a test to verify the inverter behavior if the undervoltage is cleared before the *trip delay time* of the passive anti-islanding protection (1 s).

Technical standards adopted in other countries seem to be more specific than AS 4777.2:2015 regarding the behaviour an inverter shall maintain during undervoltage, or other abnormal voltage conditions. The possible inverter behaviors are specified by voltage vs. time profiles as reported in the following paragraphs.

Technical specification IEC TS 62786-2017 has a specific section regarding immunity to grid disturbances of DER connected to the distribution network [5, Section 4.5]. In the under voltage ride-through requirements (UVRT) section is given the voltage vs. time curve in Fig. 27, which must be read in conjunction with the table given in the Annex C of the same specification, and reported in Table 15 here. Fig. 27, [5] mandates that the DER must remain connected for undervoltage falling within "Range 1", while it is allowed to disconnect for an undervoltage falling within "Range 2"

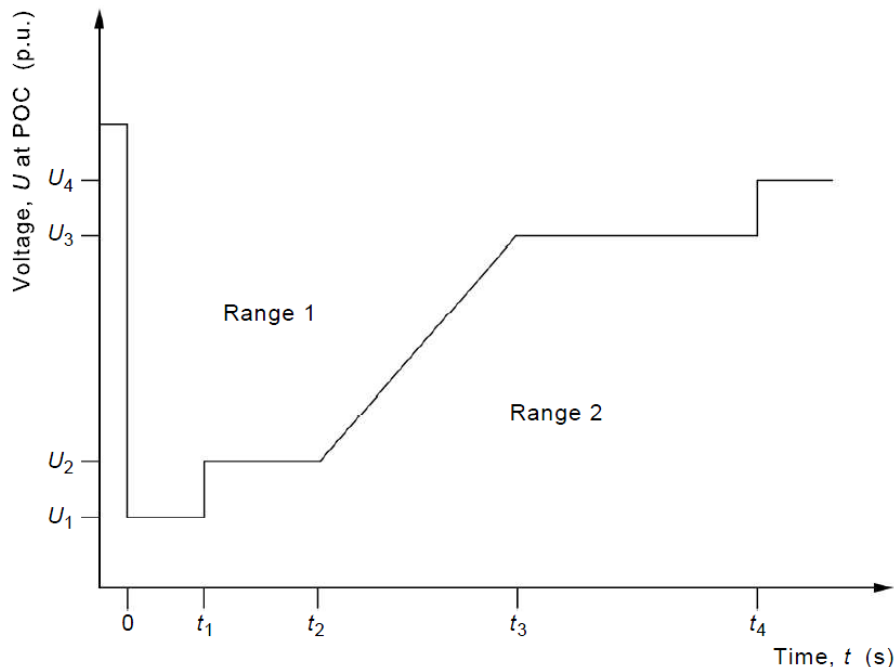


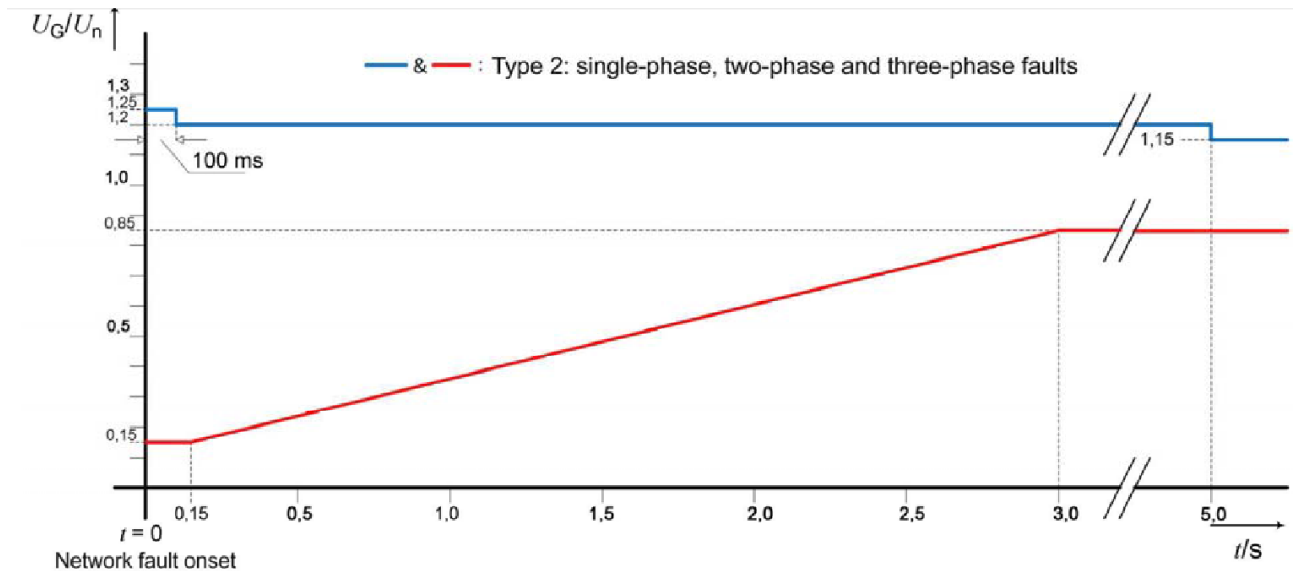
Figure 27: Undervoltage ride through capability requirement o DER [5].

Table 15: Values of voltage and time for the graph of Fig. 27 [5].

**- UVRT capability of DERs with an interface
to the grid based on non-synchronous generators
(eg. converters, DFIG, etc.)**

Parameters	Residual voltage in per unit	Ride through time in seconds
U_1, t_1	0,00 to 0,30	0,0 to 1,0
U_2, t_2	0,00 to 0,30	0,0 to 1,0
U_3, t_3	0,05 to 0,90	0,0 to 2,0
U_4, t_4	$U_{\min 2}$	0,0 to 180,0
NOTE 1	$t_1 \leq t_2 \leq t_3 \leq t_4, U_1 \leq U_2 \leq U_3 \leq U_4$.	
NOTE 2	By choosing the same values for (U_1, t_1) and (U_2, t_2) , the second data point disappears, which allows the use of the same diagram and methodology in describing the LVRT capability for both classes of generating units.	

The German standard VDE-AR-N 4105-2018 [10] mandates under voltage ride through requirements which are similar to the ones specified in [5]. The voltage vs. time curve is given in Fig. 28, where over voltage (blue line) and undervoltage (red line) ride through curves are reported.



Key

- & — FRT curve for single-phase, two-phase and three-phase network faults
UG r.m.s. value of the actual voltage at the generator terminals

Figure 28: Fault Ride-Through (FRT) limit curve for the voltage curve at the generator terminals for a type 2 power generation unit and for storage units [10, p. 37].

Moreover, the German standard states that inverters must not inject current into the grid if certain voltage conditions are met, reading [10, pp. 37-38]:

If the voltage at the generator terminals falls below $< 0.8 U_n$ or exceeds $> 1.15 U_n$ [where U_n is the rated voltage] (onset of fault), type 2 [i.e. inverter-connected] power generation units and storage units shall ride through voltage drops *without feeding current* into the network of the network operator (limited dynamic network stability).

and it continues specifying the *behaviour at the end of the fault*:

If, after the end of a fault, the network voltage resumes a value within the voltage band from $-15 \% U_n$ to $+10 \% U_n$ and the active current of the power generation unit and/or the storage unit has been reduced during the network fault, it shall, immediately after the end of the fault, be increased to its pre-fault value as quickly as possible. The transient period shall not exceed a maximum of 1 s.

The IEEE Std 1547-2015 which applies across the USA, divides DER generators based on the response they provide during abnormal conditions of the area power system [7, p. 19] to which they are connected. These are *Category I*, *Category II* and *Category III*, where it appears that a higher *Category* demands more stringent performance to the DER generators, considering that this is connected in an area with high DER penetration.

Taking for instance DER generators belonging to *Category III*, their operation during abnormal voltage conditions is defined by the table below [7, Table 16 on p. 48], where *cease to energize* means that no active power output is delivered and *momentary cessation* is a temporary *cease to energize* regime in response to a voltage or frequency disturbance, with immediate restoration of the pre-disturbance regime when voltage and frequency return within defined ranges.

Table 16 [7, Table 16 on p. 48] is read in conjunction with Fig. 29 [7, Figure H.9 on p. 134] which, similarly to the aforementioned standards, defines a voltage vs. time profile to specify the DER generator behavior in case of voltage disturbances.

Table 16: IEEE Std 1547-2015 voltage ride-through requirements for DER of abnormal operating performance Category III [7].

Voltage range (p.u.)	Operating mode/response	Minimum ride-through time (s) (design criteria)	Maximum response time (s) (design criteria)
$V > 1.20$	Cease to Energize ^a	N/A	0.16
$1.10 < V \leq 1.20$	Momentary Cessation ^b	12	0.083
$0.88 \leq V \leq 1.10$	Continuous Operation	Infinite	N/A
$0.70 \leq V < 0.88$	Mandatory Operation	20	N/A
$0.50^e \leq V < 0.70$	Mandatory Operation	10	N/A
$V < 0.50^e$	Momentary Cessation ^b	1	0.083

^aCessation of current exchange of DER with Area EPS in not more than the maximum specified time and with no intentional delay. This does not necessarily imply disconnection, isolation, or a trip of the DER. This may include momentary cessation or trip.

^bTemporarily cease to energize an EPS, while connected to the Area EPS, in response to a disturbance of the applicable voltages or the system frequency, with the capability of immediate restore output of operation when the applicable voltages and the system frequency return to within defined ranges.

^cThe voltage threshold between mandatory operation and momentary operation may be changed by mutual agreement between the Area EPS operator and DER operator, for example to allow the DER to provide Dynamic Voltage Support below 0.5 p.u.

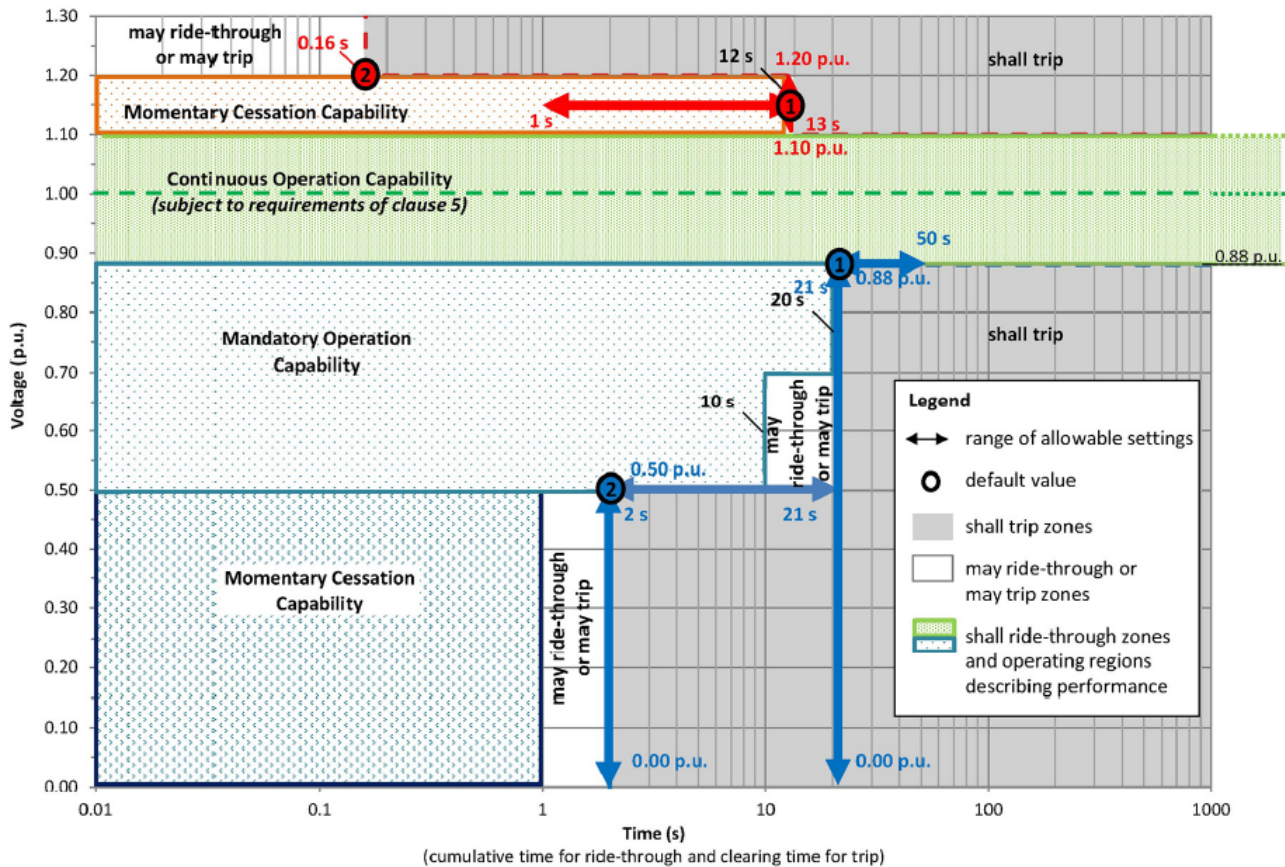


Figure 29: DER response to abnormal voltages and voltage ride-through requirements for DER of abnormal operating performance Category III [7, Figure H.9 on p. 134].

1.5.2 Phase angle jump

The bench testing process has exposed the vulnerability of certain make of inverters to (grid voltage) phase angle jumps. These phenomena can be experienced for instance by low voltage connected inverters as a consequence of faults taking place in the medium voltage network (see [9] for an in-depth review). The current version of the Australian standard AS 4777.2:2015 neither specifies the desired inverter behavior against a phase angle jumps, nor provides a procedure to test the inverter against this disturbance. Therefore a glance on international legislation can be useful. For instance, the **IEEE Std. 1547-2018** mandates that DER shall ride through voltage phase angle changes, stating [7, p. 58]:

Multi-phase DER shall ride through for positive-sequence phase angle changes within a sub-cycle-to-cycle time frame of the *applicable voltage* of less than or equal to 20 electrical degrees. In addition, multi-phase DER shall remain in operation for change in the phases angle of individual phases less than 60 electrical degrees, provided that the positive sequence angle change does not exceed the forestated criterion. Single-phase DER shall remain in operation for phase angle changes within a sub-cycle-to-cycle time frame of the *applicable voltage* of less than or equal to 60 electrical degrees. Active and reactive current oscillations in the post-disturbance period that are positively damped or momentary cessation of the DER having a maximum duration of 0.5 s shall be acceptable in response to phase angle changes.

As phase angle jumps do occur in the distribution network, it is important to enhance future versions of the Australian standard 4777 to take this disturbance into account, addressing inverter specifications and a testing procedures to ensure phase angle jump ride through.

1.5.3 Rate of Change of Frequency

The current version of AS 4777 does not mandate any RoCoF ride through for DER inverters, and in the bench-testing process it was shown that RoCoF as low as 1 Hz/s, could cause the unwanted disconnection of certain inverters from the grid. Looking at international standards, it seems that RoCoF is a recognised issue, and hence the DER inverters are required to remain connected even if experiencing a RoCoF.

IEC TS 62786-2017 specifies that “the generating unit shall be able to operate with a RoCoF as specified by individual countries” and that in some countries 2.5 Hz is required for RoCoF immunity [5, p. 13].

The German standard **VDE AR-N 4105** also includes RoCoF requirements, specifying that inverters should be able to ride through rapid frequency changes without disconnecting from the network. Precisely, it is states that the inverter should ride through RoCoF, provided that the following rates are not exceeded [7, p. 26]:

- $\pm 2.0 \text{ Hz/s}$ for a moving time slot of 0.5 s; or
- $\pm 1.5 \text{ Hz/s}$ for a moving time slot of 1 s; or
- $\pm 1.25 \text{ Hz/s}$ for a moving time slot of 2 s.

Finally, the **IEEE Std. 1547-2018** specify that *Category III* DER shall withstand RoCoF of 3.0 Hz/s [7, p. 58].

It is apparent that the RoCoF specification is part of existing advanced standards for the interconnection of DER to the distribution network, therefore it is expected that RoCoF requirements will be included in future enhanced version of the Australian standard too.

1.6 Inverters Tested and Power Percentage in the NEM

Finally, based on the power rating of the inverter tested multiplied by the number of units installed, and based on the DER power of systems up to 9.5 kW (reported in Table 3), the percentage of inverters tested in each state and in the NEM is given Table 17. Overall, the inverters tested so far, represent 9.22% of the power installed in the NEM (from PV systems of size up to 9.5 kW).

In the next year, it is planned to test more inverters according to Table 18, representing an additional 13.94% of all inverters installed in the NEM.

Table 17: Power percentage of each tested PV inverter in the National Energy Market

Inv.	Brand	Power (kW)	NSW	VIC	QLD	SA	WA	TAS	NT	NEM
1	A	4.6	0.89%	0.45%	0.82%	1.27%	0.56%	0.60%	6.69%	0.83%
2	B	4.6	0.79%	1.39%	1.01%	0.84%	0.66%	0.56%	1.57%	0.96%
3	C	4.99	1.84%	1.68%	3.11%	0.72%	1.57%	0.61%	1.29%	2.01%
4	D	4.6	0.00%	0.00%	0.00%	0.00%	0.00%	0.00%	0.00%	0.00%
5	E	5	0.90%	0.77%	3.54%	0.71%	0.37%	1.39%	0.56%	1.60%
6*	A	3	0.16%	0.06%	0.09%	0.13%	0.14%	0.08%	0.03%	0.11%
6**	A	3	0.43%	0.33%	0.35%	0.73%	0.38%	0.68%	0.15%	0.42%
7	A	4	0.10%	0.03%	0.03%	0.07%	0.02%	0.10%	0.04%	0.05%
8	A	5	0.02%	0.02%	0.05%	0.04%	0.03%	0.02%	0.02%	0.04%
9	B	3	0.03%	0.07%	0.10%	0.03%	0.07%	0.01%	0.00%	0.07%
10	F	4.6	0.00%	0.00%	0.00%	0.00%	0.00%	0.00%	0.00%	0.00%
11	D	4.2	0.01%	0.03%	0.01%	0.02%	0.01%	0.02%	0.00%	0.01%
12	D	5	0.30%	1.00%	0.50%	0.38%	0.39%	0.92%	0.00%	0.52%
13	C	4.99	0.52%	0.22%	0.51%	0.04%	0.06%	0.07%	0.14%	0.33%
14	E	5	0.54%	0.86%	4.32%	0.81%	0.55%	3.23%	0.24%	1.85%
15	G	1.5	0.00%	0.00%	0.00%	0.00%	0.00%	0.00%	0.00%	0.00%
16	D	3	0.03%	0.07%	0.03%	0.04%	0.05%	0.03%	0.00%	0.04%
17	H	4.6	0.48%	0.19%	0.64%	0.21%	0.05%	0.67%	0.03%	0.38%
TOT.	N/A	N/A	7.06%	7.18%	15.13%	6.03%	4.91%	9.00%	10.76%	9.22%

*: Inverter 6 post 2015.

**: Inverter 6 pre 2015.

Table 18: Inverters to be tested in the next stage of the project (the percentage is calculated by dividing the scaled power of each inverter by the total power in the NEM from DER sources up to 9.5 kW)

Inv.	Brand	Power (kW)	NEM	
			MW	%
18	A	4.6	174.23	2.57
1*	A	4.6	167.28	2.47
19	H	4.6	118.59	1.75
20	I	1.5	27.96	0.41
21	J	5	91.42	1.35
21	J	5	91.42	1.35
22	A	4	72.07	1.06
23	K	0.27	4.72	0.07
24	L	5	82.66	1.22
25	I	2	27.74	0.41
26	A	5	51.68	0.76
27	M	5	32.04	0.47
28	B	5	19.72	0.29
			944.94	13.94

*: Inverter 1 pre 2015.

1.7 Conclusions

The bench testing process has provided an excellent insight in understanding the response of DER inverters to grid disturbances. The tests which have been performed did not necessarily reflect those ones prescribed by the standard AS 4777.2:2015. This has allowed to identify tests which can be designed in future versions of AS 4777, to improve inverter performance and security of the electricity supply in areas with high DER penetration.

It was demonstrated that phase angle jumps in the grid voltage can cause the sudden disconnection of the inverter from the grid. When this behavior is replicated by thousands of inverters distributed in certain areas of the grid, significant load imbalances can occur, jeopardizing the stability of the system. The same conclusion can be drawn regarding the rapid voltage sag test. This has demonstrated that a voltage disturbance, clearing within the trip delay time of an inverter (1 s), can cause an unwanted disconnection of the inverter from the ac grid. The inverter ability to withstand rate of changes in the grid frequency, whose verification is not part of AS 4777, was also shown to vary across different inverter manufacturers. Two inverters from one particular manufacturer exhibited high vulnerability to this disturbance, disconnecting for rate of change of frequency as low as 1 Hz/s. Finally, the step frequency tests on AS 4777.2:2015 compliant inverters, showed that inverter from different manufacturers have very different response times, and this could be a potential issue when for instance an inverter is required to reduce its output power quickly to support restoration of the grid frequency. In AS 4777.3:2005 compliant inverters the frequency step tests have highlighted the different frequency disconnection limits across different manufacturers, presenting a challenge for creating accurate load models.

Finally, a glance at advanced international standards and specifications has highlighted that inverter ride-through against rapid voltage sags, phase angle jumps and RoCoF are well defined and mandatory in some countries. This suggests that future versions of the AS 4777 should also articulate inverter specifications to withstand these grid disturbances, as well as testing procedures to verify inverter compliance.

2 THE COMPOSITE LOAD MODEL

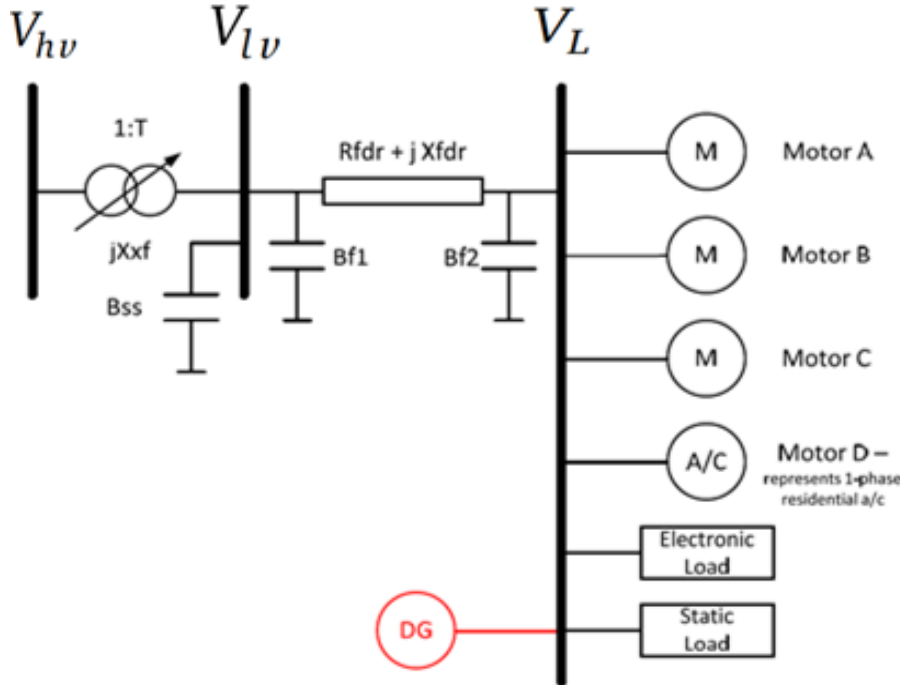


Figure 30: Diagram of the WECC Composite Load Model (WECC-CMLD).

2.1 WECC-CMLD Description

Exhaustive international work has paved the way towards the development of more precise composite load models for power system dynamic simulations. Recently, the Western Electricity Coordinating Council (WECC) proposed a generic composite load model that includes a representation of the distribution feeder, and the aggregate behaviour of various loads and DERs connected in distribution systems. A diagram of the WECC composite load model (WECC-CMLD) is depicted in Fig 30. Each component of the model can be described as follows:

- **Motor A:** Three-phase induction motor with low inertia which represents the aggregate behaviour of motors driving loads with constant torque, such as commercial and residential air conditioning and refrigerator compressors. This model should not be used to represent the dynamics of residential loads.
- **Motor B:** Three-phase induction motor with large inertia which represents the dynamics of commercial ventilation fan motors and air-handling systems.
- **Motor C:** Three-phase induction motors with low inertia driving loads whose torque is proportional to speed squared. Typically includes motors found in commercial water circulation pumps in central cooling systems

- **Motor D:** Single-phase induction motors representing primarily residential air conditioner compressor motors. In Australia, air conditioning loads might be connected to the grid via power electronic converters, this must be further investigated.
- **Power electronic loads:** Inverter-based or electronically coupled loads.
- **Static loads:** Other types of loads not explicitly modelled in the other components. Includes lighting, small electrical household and small commercial loads.

It is important to mention that the motors and the power-electronic-load components of the WECC-CMLD have an accurate model of their protection equipment (relay model for motors). This is to represent the behaviour of the devices when exposed to extreme disturbances in the power grid. When a disturbance exceeds the upper and lower limits of operation of each device, the protection equipment trips the appliance after an inherent delay. This action of the protective relay is reflected in the model by tripping the appliance from the WECC-CMLD.

One of the greatest challenges when developing the WECC-CMLD is the identification of the critical parameters of each component—specifically the load fractions and the under-voltage protection settings. One possible solution is to conduct surveys on the types of residential and commercial loads connected in various feeders of the distribution networks in Australia. Unfortunately, the parameters derived from past surveys have some degree of inaccuracy. This inherent error can be reduced by calibrating the parameters using measurement-based estimation. The measurement-based load modelling aims at deriving the load model parameters directly from disturbance measurements at different substations, times of the day, weather conditions and so on. In this section, the dynamic equations and parameters of the WECC-CMLD are described in detail. Next, in Section 3, the derived model will be used to estimate the most influential parameters using a measurement-based load modelling approach.

2.2 WECC-CMLD Equations and Parameters

This sections gives a thorough description of each load component of the WECC-CMLD. The DG component (DER_A) was explained in the Milestone 1 report.

2.2.1 Distribution Transformer and Feeder

The first component in the WECC-CMLD is the substation transformer (X_{xf}) along with an on-load tap-changer (OLTC) control, substation shunt-capacitors (B_{ss}) and the feeder inter-connecting the sub-transmission network with the distribution system. As indicated in Fig. 30, the voltage at the primary-side (or high-voltage side) of the tap changer transformer is V_{hv} and the voltage at the secondary-side (or low-voltage side) is V_{lv} . The TAP of the substation transformer is determined by the following equation [16]:

$$TAP = \sqrt{\frac{V_{hv}((V_{min} - V_{max})/2)^2}{(Q_L X_{xf} - V_{hv})^2 + (X_{xf} P_L)^2}} \quad (2)$$

where P_L and Q_L are the active and reactive power entering at the load bus. The TAP of the transformer is constrained to minimum and maximum values of T_{min} and T_{max} respectively. Additionally, the adjustment of TAP positions and its control have an inherent delay represented by parameters TD and TC respectively. Using equation 2, the voltage at the secondary winding of the tap changer V_{lv} can be determined as follows [16]:

$$V_{lv} = TAP \frac{T_{fixls}}{T_{fixhs}} (V_{hv} - j X_{xfr} T_{fixhs} I_{hs}), \quad (3)$$

where I_{hv} is the current at the primary-side of the transformer. Finally, the voltage at the load bus V_L can be calculated using V_{lv} and I_{hv} , as follows:

$$V_L = V_{lv} - (R_{fdr} + j X_{fdr})(I_{hv} T_{fixhs} / (TAP \cdot T_{fixls}) - j B_{ss} V_{lv}) \quad (4)$$

The default parameters related to each of these components are given below.

- Substation compensation B_{ss} ; pu on load base: **0**
- Rfdr - Feeder resistance; pu on load base: **0.04**
- Xfdr - Feeder reactance; pu on load base: **0.04**
- Xxf - Transformer reactance; pu on load base: **0.08**
- Tfixhs - High side fixed transformer tap: **1**
- Tfixls - Low side fixed transformer tap: **1**
- LTC - LTC flag (1=active; 0=inactive): **1**
- Tmin - LTC min tap (on low side): **0.9**
- Tmax - LTC max tap (on low side): **1.1**
- Step - LTC Tstep (on low side): **0.0063**
- Vmin - Min value of V target range on xfr low side: **1**
- Vmax - Max value of V target range on xfr low side: **1.02**
- TD - LTC control time delay; s: **30**
- TC - LTC tap adjustment time delay; s: **5**

2.2.2 Three-phase Induction Motors (Motor A, B and C)

Each induction motor $k \in \{A, B, C\}$ is represented by a set of nonlinear algebraic and differential equations. A block diagram for the model of motor k is depicted in Fig. 31. The fifth-order dynamical model for motor k is governed by vector of state variables $\mathbf{x}_k = [E'_q, E'_d, E''_q, E''_d, \omega]^T$, a vector of parameters $\mathbf{z}_k = [T'_0, T''_0, L_s, r_s, L', L'', H, E_{trq}, F_{mk}, LF]^T$, a vector of algebraic variables $\mathbf{c}_k = [i_d, i_q, Slip]^T$ and a vector of inputs $\mathbf{v}_k = [V_d, V_q]^T$. For the sake of clarity, we avoid adding the subscript k in the variables and parameters of each motor, however, we advise the reader that these variables are different for each induction motor. The parameters for three-phase induction motor k are explained below:

- F_{mk} - Motor A, B, C composite load motor fractions F_{mA}, F_{mB}, F_{mC} : **0.12, 0.14, 0.1**
- LF - Motor A, B, C real power to power base ratio: **0.75, 0.75, 0.75**
- r_s - Motor A, B, C stator resistance, pu on motor base: **0.04, 0.03, 0.03**

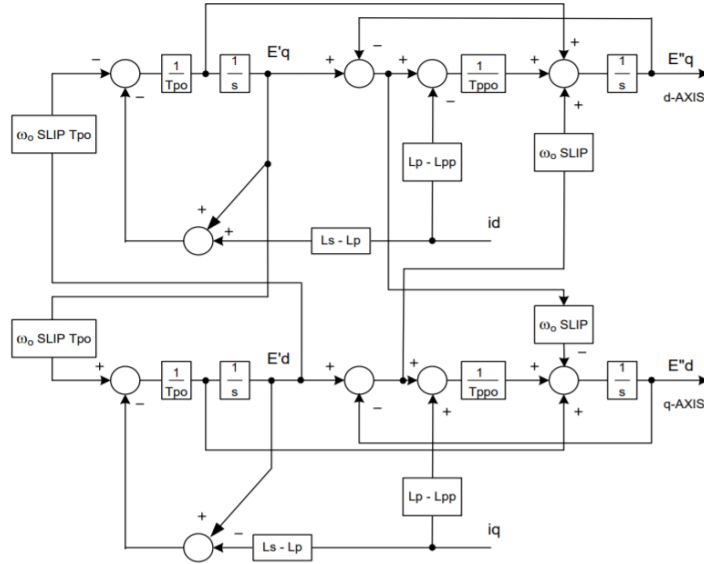


Figure 31: Block diagrams of Motor A, B and C in the WECC-CMLD [15].

- $X_s(\omega L_s)$ - Motor A, B, C synchronous reactance, pu: **1.8, 1.8, 1.8**
- $X'(\omega L')$ - Motor A, B, C transient reactance, pu: **0.12, 0.19, 0.19**
- $X''(\omega L'')$ - Motor A, B, C subtransient reactance, pu: **0.104, 0.14, 0.14**
- T'_o - Motor A, B, C transient open circuit time constant, s: **0.095, 0.2, 0.2**
- T''_o - Motor A, B, C subtransient open cir time constant, s: **0.0021, 0.0026, 0.0026**
- H - Motor A, B, C inertia constant: **0.1, 0.5, 0.1**
- E_{trq} - Motor A, B, C exponential for variation of torque with speed: **0, 2, 2**

The dynamic equations of each induction motor can be derived from the block diagram in Fig. 31, as follows:

$$\frac{dE'_q}{dt} = \frac{-1}{T'_0} E'_q - \frac{1}{T'_0} (L_s - L') i_d - \omega_0 \text{Slip} E'_d, \quad (5)$$

$$\frac{dE'_d}{dt} = \frac{-1}{T'_0} E'_d + \frac{1}{T'_0} (L_s - L') i_d + \omega_0 \text{Slip} E'_q, \quad (6)$$

$$\frac{dE''_q}{dt} = \frac{T'_0 - T''_0}{T'_0 T''_0} E'_q - \frac{E''_q}{T''_0} - \frac{(L_s - L') T''_0 + (L' - L'') T'_0}{T'_0 T''_0} i_d - \omega_0 \text{Slip} E''_d, \quad (7)$$

$$\frac{dE''_d}{dt} = \frac{T'_0 - T''_0}{T'_0 T''_0} E'_d - \frac{E''_d}{T''_0} + \frac{(L_s - L') T''_0 + (L' - L'') T'_0}{T'_0 T''_0} i_q + \omega_0 \text{Slip} E''_q. \quad (8)$$

$$\frac{d\omega}{dt} = -\frac{T_e - T_m}{2H}. \quad (9)$$

Where the electrical and mechanical variables of vector \mathbf{c}_k are given by the algebraic equations (10)-(13).

$$i_d = \frac{r_s}{r_s^2 + L''^2} (V_d + E_d'') + \frac{L''}{r_s^2 + L''^2} (V_q + E_q'') \quad (10)$$

$$i_q = \frac{r_s}{r_s^2 + L''^2} (V_q + E_q'') + \frac{L''}{r_s^2 + L''^2} (V_d + E_d'') \quad (11)$$

$$\text{Slip} = 1 - \omega \quad (12)$$

$$Tm = T_{m0}\omega^{Etrq} \quad (13)$$

Using the model in equations (5)-(13), the active and reactive power outputs of induction motor k as functions of \mathbf{x}_k , \mathbf{z}_k , \mathbf{c}_k and \mathbf{v}_k can be calculated by the following equations:

$$P_{IM,k}(\mathbf{x}_k, \mathbf{z}_k, \mathbf{c}_k, \mathbf{v}_k) = V_d i_d + V_q i_q \quad (14)$$

$$Q_{IM,k}(\mathbf{x}_k, \mathbf{z}_k, \mathbf{c}_k, \mathbf{v}_k) = V_d i_q - V_q i_d \quad (15)$$

If the input voltage in steady-state is \mathbf{v}_k^0 and the active and reactive power at the load bus are P_L and Q_L respectively (obtained from the power flow solution in steady state), induction motor k has a initial steady-state power output of:

$$P_{IM,k}(\mathbf{x}_k, \mathbf{z}_k, \mathbf{c}_k, \mathbf{v}_k^0) = F_{mk} P_L \quad (16)$$

$$Q_{IM,k}(\mathbf{x}_k, \mathbf{z}_k, \mathbf{c}_k, \mathbf{v}_k^0) = F_{mk} Q_L \quad (17)$$

Parameter F_{mk} is known as *load-fraction*; it represents the fraction of active and reactive power dragged by induction motor k in the WECC-CMLD. The load fraction F_{mk} is used to obtain the initial conditions of the state variables of each motor k . More specifically, the initial conditions are obtained by solving for i_d and i_q in equations (14) and (15) with the initial active and reactive power values in (16) and (17). Using the values derived for i_d and i_q , the initial conditions of all the state variables can be obtained by solving for the equilibrium point \mathbf{x}_k^* of equations (5)-(9) with $d\mathbf{x}_k/dt = 0$.

Motor k has a detailed model of its built-in protection equipment. The protection model has two levels of voltage tripping which can emulate a partial tripping of the motor when the terminal voltage exceeds the defined limits. The parameters of the protection mechanism are given in a user-defined parameter vector $\mathbf{z}_{prt,k} = [V_{tr1}, T_{tr1}, F_{tr1}, V_{rc1}, T_{rc1}, V_{tr2}, T_{tr2}, F_{tr2}, V_{rc2}, T_{rc2}]^T$. Each parameter is described as follows:

- V_{tr1} - Motor A, B, C 1st undervoltage trip voltage, pu: **0.65, 0.55, 0.58**
- T_{tr1} - Motor A, B, C 1st undervoltage trip delay, s: **0.1, 0.02, 0.03**
- F_{tr1} - Motor A, B, C 1st undervoltage trip fraction: **0.2, 0, 0**
- V_{rc1} - Motor A, B, C 1st undervoltage reclose voltage, pu: **0.1, 0.65, 0.68**
- T_{rc2} - Motor A, B, C 1st undervoltage reclose delay, s: **99999, 0.05, 0.05**
- V_{tr2} - Motor A, B, C 2nd undervoltage trip voltage, pu: **0.5, 0.5, 0.53**

- T_{tr2} - Motor A, B, C 2nd undervoltage trip delay, s: **0.02, 0.025, 0.03**
- F_{tr2} - Motor A, B, C 2nd undervoltage trip fraction: **0.75, 0, 0**
- V_{rc2} - Motor A, B, C 2nd undervoltage reclose voltage, pu: **0.65, 0.6, 0.62**
- T_{rc2} - Motor A, B, C 2nd undervoltage reclose delay, s: **0.1, 0.05, 0.1**

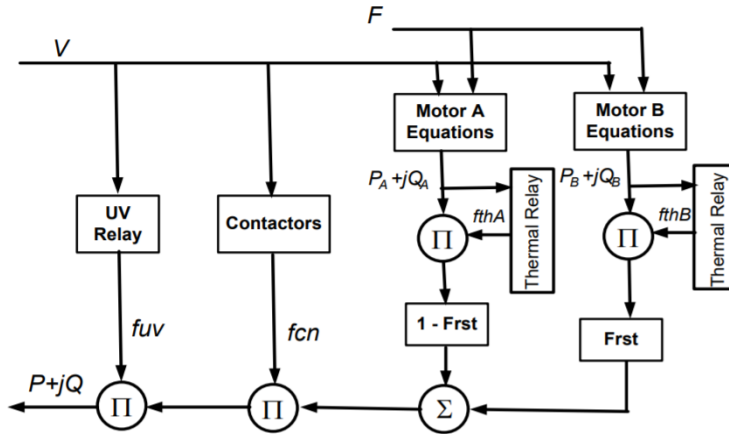


Figure 32: Block diagram of single-phase induction motor (Motor D) [15]

2.2.3 Single-Phase Induction Motor (Motor D)

This model is meant to represent the aggregate behaviour of single-phase air conditioners. A block diagram of the model for Motor D is depicted in Fig. 32. With this model, it is possible to determine the air conditioners active and reactive power and the power factor variation due to voltage and frequency disturbances. Another feature of the model is the possibility to emulate the motor stalling phenomenon. Both the motor current as well as the active and reactive power can be modelled in stalled state. Similar to the three-phase motors, partial tripping of motor D due to action of the protection equipment can be emulated by using appropriate under-voltage and thermal relay models. A brief description of each component shown in Fig. 32 will be provided below.

- **Compressor Motor Model:** This model represents the behaviour of compressor motors in both run and stall states. The model transitions from normal state to stall state if the terminal voltage is less than a user-defined stall voltage V_{stall} for an amount of time greater than T_{stall} . When the model operates in stall state, it is represented by an user-defined equivalent impedance $R_{stall} + jX_{stall}$. As shown in Fig. 32, the model is composed of two different motors, namely motor A and motor B, operating simultaneously in the simulation. Motor A represents the restartable compressor motors and B emulates the non-restartable ones. The model is mathematically represented by a vector of inputs variables $\mathbf{v}_D = [V, \omega]^T$, a vector of parameters $\mathbf{z}_D = [K_{p1}, K_{p2}, K_{q1}, K_{q2}, V_{brk}, V_{stall}, N_{p1}, N_{p2}, N_{q1}, N_{q2}, CmpK_{pf}, CmpK_{qf}, CompPF, CompLF, T_{stall}, R_{stall}, X_{stall}, T_{restart}, F_{rst}, V_{rst}, FmD]^T$. In the run state, the characteristic equations between the active/reactive power and the voltage are exponential. The active power P_D and reactive power Q_D as functions of \mathbf{v}_D and \mathbf{z}_D in the run state are expressed as follows:

$$P_D(\mathbf{v}_D, \mathbf{z}_D) = \begin{cases} P_0 + K_{p1}(V - V_{brk})^{N_{p1}} & V_{brk} \leq V \\ P_0 + K_{p2}(V - V_{brk})^{N_{p2}} & V_{stall} \leq V \leq V_{brk} \end{cases} \quad (18)$$

$$Q_D(\mathbf{v}_D, \mathbf{z}_D) = \begin{cases} Q_0 + K_{q1}(V - V_{brk})^{N_{q1}} & V_{brk} \leq V \\ Q_0 + K_{q2}(V - V_{brk})^{N_{q2}} & V_{stall} \leq V \leq V_{brk} \end{cases} \quad (19)$$

Where P_0 and Q_0 are obtained at $V = 1$ p.u, as follows:

$$P_0 = F_{mD} P_L - K_{p1} (1 - V_{brk})^{N_{p1}}, \quad (20)$$

$$Q_0 = F_{mD} Q_L - K_{q1} (1 - V_{brk})^{N_{q1}}, \quad (21)$$

Where F_{mD} is the load fraction assigned to motor D. In order to emulate frequency dependency of the model, the active and reactive power in (18) and (19) are modified as follows:

$$P_D(\mathbf{v}_D, \mathbf{z}_D) \leftarrow P_D(\mathbf{v}_D, \mathbf{z}_D)(1 + CmpK_{pf} \frac{\omega - \omega_0}{2\pi}) \quad (22)$$

$$Q_D(\mathbf{v}_D, \mathbf{z}_D) \leftarrow Q_D(\mathbf{v}_D, \mathbf{z}_D)(1 + \frac{CmpK_{qf}(\omega - \omega_0)}{(1 - CompPF^2)2\pi}) \quad (23)$$

The parameters related to the compressor motor model as explained below:

- FmD - Composite load motor D fraction: **0.03**
- Tstall - Motor D stall delay time, s: **0.03**
- Trestart - Motor D restart from stall delay time, s: **0.3**
- ComplF - Motor D real power to motor base ratio: **1**
- CompPF - Motor D power factor at 1.0 pu voltage: **0.98**
- Vstall - Motor D stall Voltage, pu: **0.45**
- Rstall - Motor D stall resistance, pu of motor base: **0.1**
- Xstall - Motor D stall reactance, pu of motor base: **0.1**
- LFadj - Adjustment to stall voltage if COMPLF /= 1.0: **0**
- Kp1 - Motor D real power coeff when voltage > Vbrk: **0**
- Np1 - Motor D real power exp when voltage > Vbrk: **1**
- Kq1 - Motor D reactive power coeff when voltage > Vbrk: **6**
- Nq1 - Motor D reactive power exp when voltage > Vbrk: **2**
- Kp2 - Motor D real power coeff when voltage < Vbrk: **12**
- Np2 - Motor D real power exp when voltage < Vbrk: **3.2**
- Kq2 - Motor D reactive power coeff when voltage < Vbrk: **11**
- Nq2 - Motor D reactive power exp when voltage < Vbrk: **2.5**
- Vbrk - Motor D "break-down" voltage,: **0.86**
- Frst - Motor D fraction capable of restart after stall: **0.2**
- Vrst - Motor D voltage for restart after stall, pu: **0.95**
- CmpKpf - Motor D real power frequency dependency: **1**
- CmpKqf - Motor D reactive power freq dependency: **-3.3**

- **Contactor Model** Power contactors are used to energize the compressor motors. The status of the power contactor (1 or 0) depends entirely on the input voltage V . The input voltage V and frequency f are estimated using first-order lag filters with time constants T_v and T_f respectively. The parameters of the power contactor are given in vector $\mathbf{z}_{D,cnt} = [T_v, T_f, Vc1off, Vc2off, Vc1on, Vc2on]^T$. These parameters are explained below:
 - T_v - Motor D voltage time constant for contactors, s: **0.025**
 - T_f - Motor D frequency time constant for contactors, s: **0.1**
 - $Vc1off$ - Motor D voltage contactors start opening, pu: **0.5**
 - $Vc2off$ - Motor D voltage all contactors opened, pu: **0.4**
 - $Vc1on$ - Motor D voltage contactors start closing, pu: **0.6**
 - $Vc2on$ - Motor D voltage all contactors closed, pu: **0.52**
- **Under-voltage Relay Model:** If the terminal voltage exceeds the voltage thresholds for a specified amount of time, the motors are tripped from the simulation without re-connection. The under-voltage relay parameters are represented by vector $\mathbf{z}_{D,uv} = [F_{uvr}, UV_{tr1}, T_{tr1}, UV_{tr2}, T_{tr2}]^T$ and can be described as follows:
 - F_{uvr} - Motor D fraction with undervoltage relays: **0.1**
 - UV_{tr1} - Motor D 1st undervoltage pick-up, pu: **0.5**
 - T_{tr1} - Motor D 1st undervoltage trip delay, s: **0.02**
 - UV_{tr2} - Motor D 2nd undervoltage pick-up, pu: **0.1**
 - T_{tr2} - Motor D 2nd under voltage trip delay, s: **9999** s
- **Thermal Relay Model:** Air-conditioners are protected against over-heating using thermal relays. The winding temperature T_w can be calculated by equation (24), where i_c is the motor current, R_{stall} is the stall resistance and T_{th} is the motor heating time constant.

$$\frac{dT_w}{dt} = -\frac{1}{T_{th}}(i_c^2 * R_{stall} - T_w) \quad (24)$$

The thermal relay model emulates motor tripping by multiplying the active and reactive power of the motor by a fraction $0 \leq K \leq 1$. Using the computed winding temperature T_w , the model determines the value of K by comparing T_w with two user-defined parameters Th_{1t} and Th_{2t} . If $T_w < Th_{1t}$ then $K = 1$, otherwise, K is determined by linear interpolation between points $(1, Th_{1t})$ and $(0, Th_{2t})$. The thermal relay state variables parameters are represented by vectors $\mathbf{x}_{TR} = [T_w]$ and $\mathbf{z}_{D,tr} = [Th_{1t}, Th_{2t}]^T$ respectively.

The default values of the parameters of the thermal relay model are summarized as follows:

- T_{th} - Motor D heating time constant, s: **15**
- Th_{1t} - Motor D temperature where tripping begins, pu: **0.7**
- Th_{2t} - Motor D temperature where completely tripped: **1.9**

2.2.4 Electronic Loads

These loads are represented as constant active and reactive power when the terminal voltage V is greater than an user-defined voltage threshold V_{d1} . Both the active and reactive power are linearly decreased to zero if $V_{d2} \leq V \leq V_{d1}$. Voltage V_{d2} is a second user-defined voltage threshold that

indicates the minimum voltage at which electronic loads remain connected. The input of the electronic loads is the vector $\mathbf{v}_{el} = [V]$ and parameters are placed in vector $\mathbf{z}_{el} = [V_{d1}, V_{d2}, F_{el}, PF_{el}]^T$, where F_{el} and PF_{el} are the load fraction and the power factor of the electronic loads respectively. That being said, the electronic loads consume an active and reactive of:

$$P_{el}(\mathbf{v}_{el}, \mathbf{z}_{el}) = \begin{cases} F_{el} \sqrt{P_L^2 + Q_L^2} PF_{el} & V_{d1} \leq V \\ F_{el} \frac{\sqrt{P_L^2 + Q_L^2} PF_{el}}{V_{d1} - V_{d2}} (V - V_{d2}) & V_{d2} \leq V \leq V_{d1} \\ 0 & V \leq V_{d2} \end{cases} \quad (25)$$

$$Q_{el}(\mathbf{v}_{el}, \mathbf{z}_{el}) = \begin{cases} F_{el} \sqrt{P_L^2 + Q_L^2} \sin(\arccos(PF_{el})) & V_{d1} \leq V \\ F_{el} \frac{\sqrt{P_L^2 + Q_L^2} \sin(\arccos(PF_{el}))}{V_{d1} - V_{d2}} (V - V_{d2}) & V_{d2} \leq V \leq V_{d1} \\ 0 & V \leq V_{d2} \end{cases} \quad (26)$$

The default values of the parameters of the electronic load model are summarized as follows:

- Fel - Composite load electronic fraction: **0.27**
- PFel - Electronic load power factor: **1**
- Vd1 - Voltage electronic loads start to drop: **0.7**
- Vd2 - Voltage all electronic load has dropped: **0.5**

2.2.5 Static Loads

The active and reactive power of the static loads vary exponentially with respect to the input voltage V and linearly with respect to the load bus frequency f . The static load input vector is $\mathbf{v}_{st} = [V, \omega]^T$ and the parameter vector is $\mathbf{z}_{st} = [PF_s, P_{1e}, P_{1c}, P_{2e}, P_{2c}, Q_{1e}, Q_{2e}, Q_{1c}, Q_{2c}, P_{frq}, Q_{frq}]^T$. The equations of active power (P_{ST}) and reactive power (Q_{ST}) of the static loads with respect to the inputs \mathbf{v}_{st} and the parameters \mathbf{z}_{st} are given by:

$$P_{ST}(\mathbf{v}_{st}, \mathbf{z}_{st}) = P_0 \left(P_{1c} \left(\frac{V}{V_0} \right)^{P_{1e}} + P_{2c} \left(\frac{V}{V_0} \right)^{P_{2e}} + P_3 \right) (1 + P_{frq}(\omega - \omega_0)/(2\pi)), \quad (27)$$

$$Q_{ST}(\mathbf{v}_{st}, \mathbf{z}_{st}) = Q_0 \left(Q_{1c} \left(\frac{V}{V_0} \right)^{Q_{1e}} + Q_{2c} \left(\frac{V}{V_0} \right)^{Q_{2e}} + Q_3 \right) (1 + Q_{frq}(\omega - \omega_0)/(2\pi)), \quad (28)$$

where P_0 , Q_0 , P_3 and Q_3 are given by:

$$P_0 = P_L (1 - F_{mA} - F_{mB} - F_{mC} - F_{mD} - F_{el}) \quad (29)$$

$$Q_0 = Q_L (1 - F_{mA} - F_{mB} - F_{mC} - F_{mD} - F_{el}) \quad (30)$$

$$P_3 = 1 - P_{1c} - P_{2c} \quad (31)$$

$$Q_3 = 1 - Q_{1c} - Q_{2c} \quad (32)$$

The parameters of the static loads and their default values are summarized as follows:

- PFs - Static load lower factor: **1**

- P1e - First exponent for static load P: **1**
- P1c - First coeff for static load P: **0.48**
- P2e - Second exponent for static load P: **2**
- P2c - Second coeff for static load P: **0.52**
- Pfrq - Frequency sensitivity for static P: **0**
- Q1e - First exponent for static load Q: **1**
- Q1c - First coeff for static load Q: **0.48**
- Q2e - Second exponent for static load Q: **2**
- Q2c - Second coeff for static load Q: **0.52**
- Qfrq - Frequency sensitivity for static load Q: **-1**

2.3 Final WECC-CMLD States, Variables and Parameters

Based on the above discussion, the entire WECC-CMLD can be represented by a set of differential and algebraic equations. Let the state variable vector, parameter vector, algebraic variable vector and input vector of the entire WECC-CMLD be $\mathbf{x} = [\mathbf{x}_A^T, \mathbf{x}_B^T, \mathbf{x}_C^T, \mathbf{x}_{TR}^T]^T$, $\mathbf{z} = [\mathbf{z}_A^T, \mathbf{z}_{prt,A}^T, \mathbf{z}_B^T, \mathbf{z}_{prt,B}^T, \mathbf{z}_C^T, \mathbf{z}_{prt,C}^T, \mathbf{z}_D^T, \mathbf{z}_{D,cnt}^T, \mathbf{z}_{D,uv}^T, \mathbf{z}_{D,tr}^T, \mathbf{z}_{el}^T, \mathbf{z}_{st}^T]^T$, $\mathbf{c} = [\mathbf{c}_A^T, \mathbf{c}_B^T, \mathbf{c}_C^T]^T$ and $\mathbf{v} = [\mathbf{v}_A^T, \mathbf{v}_B^T, \mathbf{v}_C^T, v_D^T, \mathbf{v}_{el}^T, \mathbf{v}_{st}^T]^T$ respectively. The WECC-CMLD can be represented by the following equations:

$$\frac{d\mathbf{x}}{dt} = F(\mathbf{x}, \mathbf{z}, \mathbf{c}, \mathbf{v}), \quad (33)$$

$$0 = G(\mathbf{z}, \mathbf{c}, \mathbf{v}), \quad (34)$$

where function F contains equations (5)-(9) and equation (24) for all motors A, B, C and D. Function G is derived from equations (10)-(13) for all three induction motors. The outputs of the WECC-CMLD are the total active and reactive power consumed by all the components in the model, expressed as functions of time t , \mathbf{x} , \mathbf{z} , \mathbf{c} , \mathbf{v} in the following manner:

$$P_{cmld}(t, \mathbf{x}, \mathbf{z}, \mathbf{c}, \mathbf{v}) = P_{IM,A} + P_{IM,B} + P_{IM,C} + P_D + P_{el} + P_{ST} \quad (35)$$

$$Q_{cmld}(t, \mathbf{x}, \mathbf{z}, \mathbf{c}, \mathbf{v}) = Q_{IM,A} + Q_{IM,B} + Q_{IM,C} + Q_D + Q_{el} + Q_{ST} \quad (36)$$

3 WECC-CMLD PARAMETER DERIVATION

In power system load modelling, there are two main approaches to determine the parameters of the selected load model [11]: i) The component-based approach (see [12]) and ii) The measurement-based approach (see [13]). Both of these methods have advantages and disadvantages, therefore, in this deliverable, we take the advantages of both methods and use a hybrid approach to determine the parameters of the WECC-CMLD.

3.1 Component-based approach

The component-based load modelling aggregates the distribution of loads according to standard load classes and the load components of each class. In this approach, except for the load fractions, the parameters associated with each load component in the WECC-CMLD are fixed. Parameters are conventionally obtained based on past surveys or by averaging the values obtained from laboratory tests of common electrical appliances in residential, commercial and industrial facilities. The load fractions vary based on climate zones, seasons, time of the day and past surveys on the load composition in each of the created zone. The AEMO staff has made intensified efforts provide a rough estimation of the load composition (and the load fractions $F_{mA}, F_{mB}, F_{mC}, F_{mD}, F_{el}$) per state for winter and summer seasons. The derived load compositions are shown in Table 19 and Table 20. The remaining parameters, related to the transformer and distribution feeder (Section 2.2.1), induction motor A, B, C and D dynamics and protection (Section 2.2.2 and 2.2.3), power electronic loads (Section 2.2.4) and static loads (Section 2.2.5) are derived using previous studies on laboratory tests on different electrical devices for residential and commercial facilities.

Table 19: Load fractions obtained by AEMO (summer peak)

State	Motor A F_{mA}	Motor B F_{mB}	Motor C F_{mC}	Motor D F_{mD}	Electronic Load F_{el}
QLD	0.12	0.14	0.10	0.03	0.27
NSW	0.12	0.10	0.09	0.06	0.24
VIC	0.12	0.10	0.06	0.06	0.26
SA	0.09	0.13	0.11	0.05	0.35
TAS	0.14	0.12	0.13	0.03	0.15

Table 20: Load fractions obtained by AEMO (winter peak)

State	Motor A F_{mA}	Motor B F_{mB}	Motor C F_{mC}	Motor D F_{mD}	Electronic Load F_{el}
QLD	0.06	0.12	0.11	0.03	0.19
NSW	0.04	0.08	0.08	0.06	0.20
VIC	0.04	0.08	0.07	0.06	0.20
SA	0.05	0.12	0.11	0.06	0.26
TAS	0.08	0.11	0.11	0.04	0.15

3.2 Measurement-based approach

The component-based load model gives us a first estimation of the values of the parameters used in the WECC-CMLD. Nevertheless, due to the different types of electrical appliances connected in distribution networks, changes in weather conditions and the distinct topological structure of distribution systems, these parameters are subjected to inaccuracies. If the parameters obtained using

the component-based approach are given in vector $\mathbf{z}_0 \in \mathbb{R}^{N \times 1}$, we assume that each entry $z_i \in \mathbf{z}_0$ has an inherent error ϵ_i , and the actual parameter may fluctuate between $[z_i - \epsilon_i, z_i + \epsilon_i]$. With this in mind, the problem now is to estimate each $z_i \in [z_i - \epsilon_i, z_i + \epsilon_i]$ as to minimize the error between the active and reactive power of the WECC-CMLD and the active and reactive power obtained from measurements at each load bus.

We assume that the inputs (voltage and frequency at the load bus) and outputs (active and reactive power at the load bus) of the model in (33) and (34) are measured and represented by $\hat{\mathbf{v}}(t)$, $\hat{P}(t)$ and $\hat{Q}(t)$. The active and reactive power of the model at time t are given in equations (35) and (36). The model parameters $z_i \in \mathbf{z}$ can be estimated by minimizing the error between the model output and the measurements by solving the following non-linear optimization problem:

$$\min_{\mathbf{z} \in \mathbb{R}^{N \times 1}} J(\mathbf{z}) = \int_{t_0}^{t_f} w_p \left(\hat{P}(t) - P_{cmld}(t, \mathbf{x}, \mathbf{z}, \mathbf{c}, \hat{\mathbf{v}}(t)) \right)^2 dt + \int_{t_0}^{t_f} w_q \left(\hat{Q}(t) - Q_{cmld}(t, \mathbf{x}, \mathbf{z}, \mathbf{c}, \hat{\mathbf{v}}(t)) \right)^2 dt \quad (37a)$$

subject to $\mathbf{z}_0 - \epsilon \leq \mathbf{z} \leq \mathbf{z}_0 + \epsilon$, (37b)

$$\mathbf{A}_{eq}\mathbf{z} = \mathbf{z}_0 \quad (37c)$$

$$\mathbf{A}_{ineq}\mathbf{z} \leq \mathbf{b}_{ineq} \quad (37d)$$

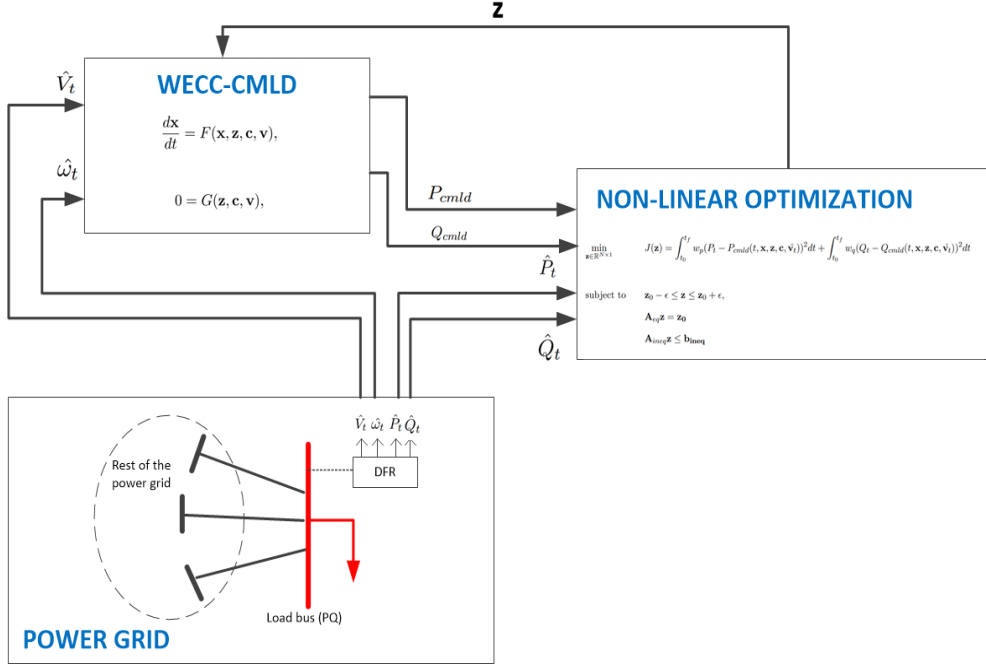


Figure 33: Developed measurement-based load model tool.

The optimization problem consists of its objective function $J(\mathbf{z})$ in (37a), which represents the error between the output and the measurement data, a set of box constraints (37b), a set of equality constraints (37c) and a set of inequality constraints (37d). The variables w_p and w_q are user-defined weights assigned to active and reactive power. These weights represent the level of importance assigned to the active and reactive power outputs. The objective function consists of a system of non-linear differential and algebraic equations. The evaluation of the objective function requires a computationally expensive numerical integration method along with a Newton-Raphson algorithm to

solve the network equations. Considering all parameters of the WECC-CMLD in the optimization problem (37a) is computationally unfeasible. Consequently, a hybrid approach is followed in this deliverable. The approach consists of selecting a subset of parameters of the WECC-CMLD to be calibrated using measurement data. The remaining parameters are constants and their values are derived using the component-based approach (this can be done using the matrix $\mathbf{A}_{eq} \in \mathbb{R}^{N \times N}$ to add equality constraints on the fixed parameters in (37c)). One inequality constraint is added using matrix $\mathbf{A}_{ineq} \in \mathbb{R}^{1 \times N}$ and vector $\mathbf{b}_{ineq} \in \mathbb{R}^{1 \times 1}$ in equation (37d). This inequality constraint forces the summation of the load fraction parameters to be less than one ($F_{mA} + F_{mB} + F_{mC} + F_{mD} + F_{el} \leq 1$). The developed measurement-based load model is shown in Fig. 33.

3.3 Parameter Estimation Solution

3.3.1 Solution algorithm

The parameter estimation problem in equations (37a)-(37d) is solved using a Sequential Quadratic Programming (SQP) algorithm. SQP is one of the most powerful iterative algorithms for non-linear gradient-based optimization problems. An efficient implementation of the SQP algorithm in FORTRAN language [1] (also available in `scipy.optimize` by means of a PYTHON wrapper) is used in this deliverable.

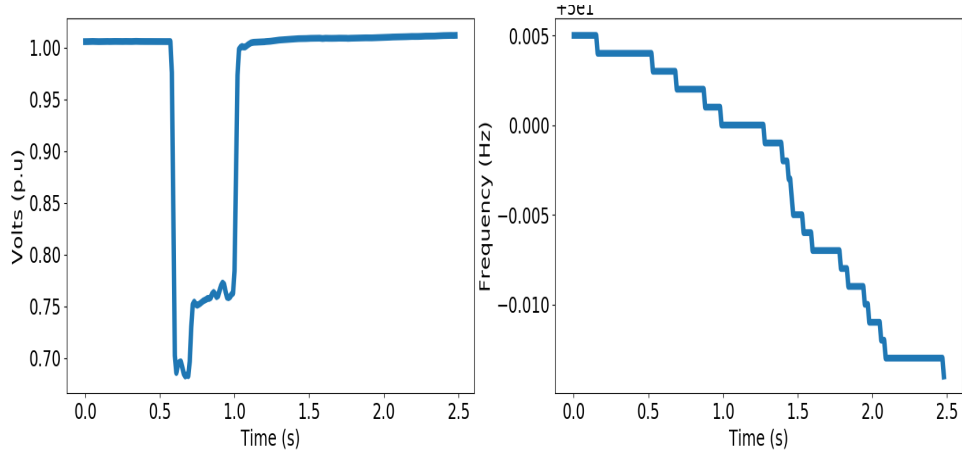


Figure 34: Feeder X event on October 21 2018 at 14:38.

3.3.2 Estimation I:

In this first experiment, we attempt to estimate 16 parameters—including the load fractions and the parameters of the static loads. All other parameters remain unchanged from their component-based default values (\mathbf{z}_0) provided in Section 2. The parameters considered in the optimization problem (37a)-(37d) are: $F_{mA}, F_{mB}, F_{mC}, F_{mD}, F_{el}, \mathbf{PFs}, P_{1e}, P_{1c}, P_{2e}, P_{2c}, P_{frq}, Q_{1e}, Q_{1c}, Q_{2e}, Q_{2c}, Q_{freq}$. The selected disturbance occurred at Feeder X on October 21, 2018 at 14:38:46. The voltage \hat{V}_t and frequency $\hat{\omega}_t$ measurements captured by the DFR are depicted in Fig. 34. In this event, the objective function in (37a) using default parameters was found to be $J(\mathbf{z}_0) = 5.416$. The upper and lower bounds in (37b) for each parameter $z_i \in \mathbf{z}$ are $z_{0,i} + 0.25|z_{0,i}|$ and $z_{0,i} - 0.25|z_{0,i}|$ respectively— $z_{0,i} \in \mathbf{z}_0$ is the component-based default value of parameter i . As mentioned, one inequality constraint forces the summation of all load fractions to be less than one.

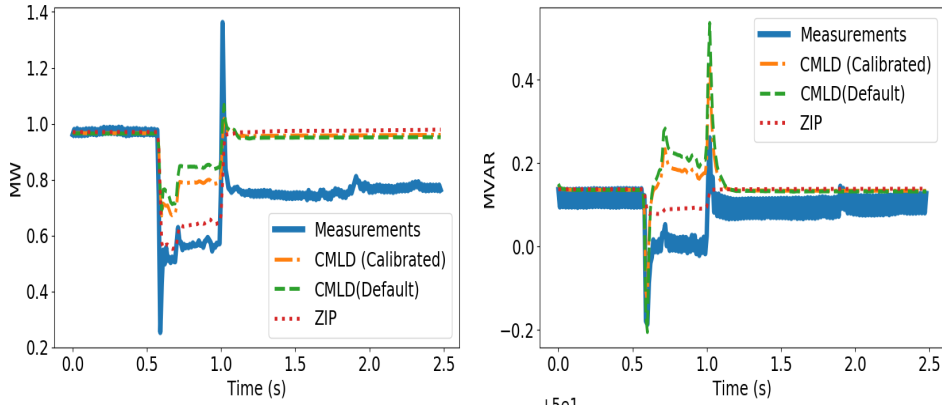


Figure 35: Estimation I: Active and reactive power outputs

The SQP algorithm is used to minimize function $J(\mathbf{z})$ in an iterative manner. The algorithm converges in 7 iterations and the results of each iteration are given in Table 21 and Table 22. The value of $J(\mathbf{z})$ at every iteration is given in the last column of Table 22. As observed, $J(\mathbf{z})$ decreases from its initial value of 5.416 to the last value of 4.231. The WECC-CMLD outputs—with the default and calibrated parameters given in the first and last row of Tables 21 and 22 respectively—are depicted in Fig. 35. The results in Fig. 35 suggest that the selected parameters are unable to significantly reduce the error between the model outputs and the measurements. It is also observed that none of the models can emulate the observed reduction in active and reactive power after the fault is cleared.

Table 21: Estimation I: Parameters in each iteration

Iter	F_{mA}	F_{mB}	F_{mC}	F_{mD}	F_{el}
1	0.120	0.140	0.100	0.030	0.270
2	0.090	0.105	0.075	0.023	0.203
3	0.090	0.105	0.075	0.022	0.203
4	0.090	0.105	0.075	0.023	0.203
5	0.090	0.105	0.075	0.022	0.203
6	0.090	0.105	0.075	0.023	0.203
7	0.090	0.105	0.075	0.023	0.203

Table 22: Estimation I: Parameters in each iteration and objective function value

Iter	PFs	P_{1e}	P_{1c}	P_{2e}	P_{2c}	P_{frq}	Q_{1e}	Q_{1c}	Q_{2e}	Q_{2c}	Q_{freq}	$J(\mathbf{z})$
1	1.000	1.000	0.480	2.000	0.520	0.000	1.000	0.480	2.000	0.520	-1.000	5.416
2	0.990	1.250	0.600	2.347	0.650	0.000	1.043	0.573	2.041	0.650	-1.005	4.306
3	0.977	1.250	0.600	2.500	0.650	0.000	1.105	0.600	2.091	0.650	-1.007	4.268
4	0.960	1.250	0.600	2.500	0.650	0.000	1.206	0.600	2.170	0.650	-1.007	4.252
5	0.960	1.250	0.600	2.500	0.650	0.000	1.250	0.600	2.298	0.650	-1.000	4.242
6	0.960	1.250	0.600	2.500	0.650	0.000	1.250	0.600	2.500	0.650	-0.995	4.231
7	0.960	1.250	0.600	2.500	0.650	0.000	1.250	0.600	2.500	0.650	-0.995	4.231

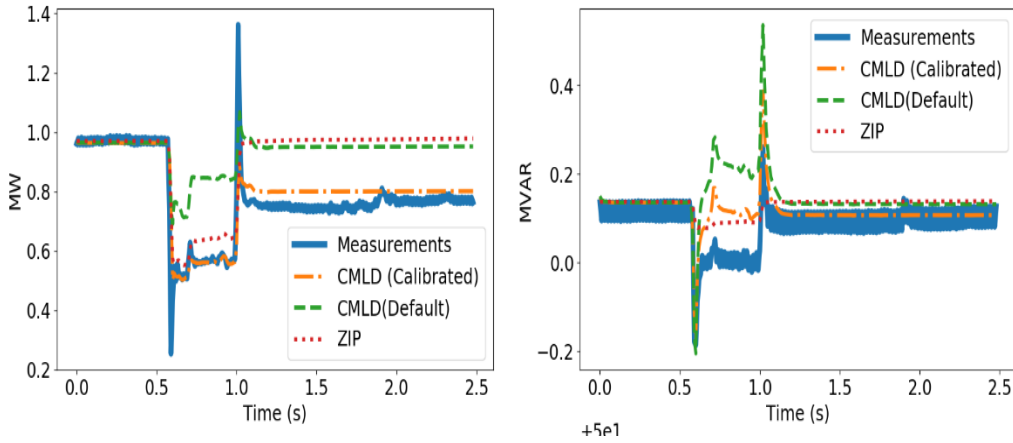


Figure 36: Estimation II: Active and reactive power outputs.

3.3.3 Estimation II

The reduction in active and reactive power observed in Fig. 35 is related to load tripping due to the action of the protection equipment of different appliances connected in the faulted feeder. Unfortunately, the default parameters assigned to the protection equipment of the different components in the WECC-CMLD cannot capture the load tripping behaviour for this disturbance. Therefore, the parameters of the protection equipment should be considered in the optimization problem (37a). In order to determine which protection parameters should be included in the error minimization problem, a sensitivity analysis was conducted. The sensitivity of the objective function $J(\mathbf{z})$ with respect to parameter z_i is calculated as $\frac{\partial J(\mathbf{z})}{\partial z_i}$. The most sensitive parameters were found to be: i) The first load tripping fraction of motor B (F_{tr1B}), ii) the first under-voltage tripping value of motor C (V_{tr1C}), iii) the first load tripping fraction of motor C (F_{tr1C}), iv) the fraction of power electronic loads that can recover (F_{reel}), v) the voltage at which electronic loads start to drop (V_{d1}) and vi) the voltage at which all the electronic loads have dropped (V_{d2}). These protection parameters, together with the ones used in Estimation I, are calibrated in this experiment.

The optimization problem now has 22 variables in vector \mathbf{z} . The upper and lower bounds are identical to the ones indicated in Estimation I and the inequality constraint on the summation of the load fraction is maintained. The SQP algorithm converges in 18 iterations. The values of the calibrated parameters during the first and last five iterations are given in Table 23 and Table 24. The value of the objective function $J(\mathbf{z})$ is given in the last column of Table 24. It is observed that $J(\mathbf{z})$ decreases from its initial value of 5.416 to its final value of 0.829. The active and reactive power outputs of the model with default and calibrated parameters are depicted in Fig. 36. As observed in this last figure, the WECC-CMLD clearly resembles the trajectory of the measurements for active and reactive power. This is because the protection parameters have been calibrated to emulate the under-voltage load tripping behaviour. Unfortunately, a small error is observed in the reactive power output at $0.6s < t < 0.9s$.

Table 23: Estimation II: Parameters and objective function

Iter.	F_{mA}	F_{mB}	F_{mC}	F_{mD}	F_{el}	V_{d1}	V_{d2}	P_{Fs}	P_{1e}	P_{1c}	P_{2e}
1	0.120	0.140	0.100	0.030	0.270	0.700	0.500	1.000	1.000	0.480	2.000
2	0.090	0.105	0.075	0.022	0.203	0.840	0.800	0.990	1.250	0.600	2.347
3	0.090	0.105	0.075	0.022	0.337	0.840	0.800	0.990	1.250	0.600	2.338
4	0.150	0.157	0.125	0.037	0.337	0.554	0.800	0.990	0.952	0.360	1.962
5	0.150	0.175	0.125	0.037	0.337	0.809	0.517	0.960	0.750	0.360	1.738
14	0.090	0.105	0.075	0.022	0.337	0.836	0.741	0.960	0.750	0.461	1.928
15	0.090	0.105	0.075	0.022	0.337	0.837	0.745	0.960	0.750	0.402	1.843
16	0.090	0.105	0.075	0.022	0.337	0.837	0.744	0.960	0.751	0.392	1.824
17	0.090	0.105	0.075	0.023	0.338	0.838	0.737	0.960	0.750	0.360	1.707
18	0.090	0.105	0.075	0.023	0.338	0.838	0.736	0.960	0.776	0.387	1.694

Table 24: Estimation II (cont.): Parameters and objective function.

Iter.	P_{2c}	P_{frq}	Q_{1e}	Q_{1c}	Q_{2e}	Q_{2c}	Q_{frq}	F_{tr1B}	V_{tr1c}	F_{tr2C}	F_{rcel}	$J(\mathbf{z})$
1	0.520	0.000	1.000	0.480	2.000	0.520	-1.000	0.000	0.580	0.000	0.800	5.416
2	0.650	0.000	1.043	0.573	2.041	0.650	-1.005	0.050	0.600	0.200	0.500	1.771
3	0.650	0.000	1.071	0.600	2.062	0.650	-1.007	0.050	0.600	0.200	0.500	1.101
4	0.390	0.000	1.181	0.600	2.142	0.650	-1.010	0.050	0.600	0.200	0.500	7.735
5	0.390	0.000	1.160	0.600	2.123	0.650	-1.006	0.050	0.600	0.200	0.500	3.190
14	0.390	0.000	1.250	0.600	2.500	0.650	-1.006	0.050	0.600	0.200	0.500	0.831
15	0.390	0.000	1.250	0.600	2.500	0.650	-1.008	0.050	0.600	0.200	0.500	0.830
16	0.390	0.000	1.250	0.600	2.500	0.650	-1.008	0.050	0.600	0.200	0.500	0.829
17	0.390	0.000	1.250	0.600	2.500	0.650	-1.007	0.050	0.600	0.200	0.500	0.829
18	0.390	0.000	1.250	0.600	2.500	0.650	-1.005	0.050	0.600	0.200	0.500	0.829

Table 25: Estimation III: Solution when extending the upper and lower bounds of the parameters

Parameter	Lower Bound	Upper Bound	Default	Calibrated
F_{mA}	0	0.3	0.12	0.231
F_{mB}	0	0.3	0.14	0.000
F_{mC}	0	0.3	0.1	0.000
F_{mD}	0	0.1	0.03	0.000
F_{el}	0.203	0.7	0.27	0.403
V_{d1}	0.3	0.84	0.7	0.840
V_{d2}	0.2	0.8	0.5	0.739
P_{Fs}	0.96	0.99	1	0.960
P_{1c}	0.15	0.6	0.48	0.150
P_{2c}	0.15	0.8	0.52	0.150
P_{frq}	0	2	0	1.047
Q_{1c}	0.1	1.8	0.48	1.800
Q_{2c}	0.3	1.5	0.52	1.500
Q_{frq}	-1.2	-0.8	-1	-1.005
F_{tr1}	0.05	0.6	0	0.550
V_{tr1}	0.5	0.8	0.58	0.620
F_{tr2}	0.2	0.9	0	0.759
F_{rcel}	0.5	0.96	0.8	0.500
$J(z)$	0	Inf	5.416	0.483

3.3.4 Estimation III

In the previous two estimations, we calibrated all static load parameters in the optimization process. The physical interpretation of static loads, however, is to represent loads with constant impedance and constant current. Constant current loads are represented by $P_{1e} = Q_{1e} = 1$ and constant impedance loads are emulated using $P_{2e} = Q_{2e} = 2$. Although the user can modify these four parameters, in order to preserve their physical meaning, we will keep them as constants in this numerical experiment. In addition, aiming to further reduce the value of the objective function, we will extend the upper and lower bounds of the remaining parameters in the calibration process. The selected bounds of each parameter are given in second and third columns of Table 25. The default and calibrated values of each parameter after convergence of the SQP algorithm are given in the fifth and sixth columns of the same table respectively. The last row of Table 25 indicates that, by allowing the parameters to change in a wider range, function $J(z)$ can be minimized to 0.483. A comparison between the output of the model and the measurements is given in Fig. 37, where both the active and reactive power now resemble the trajectory of the measurements more accurately than the previous two estimations.

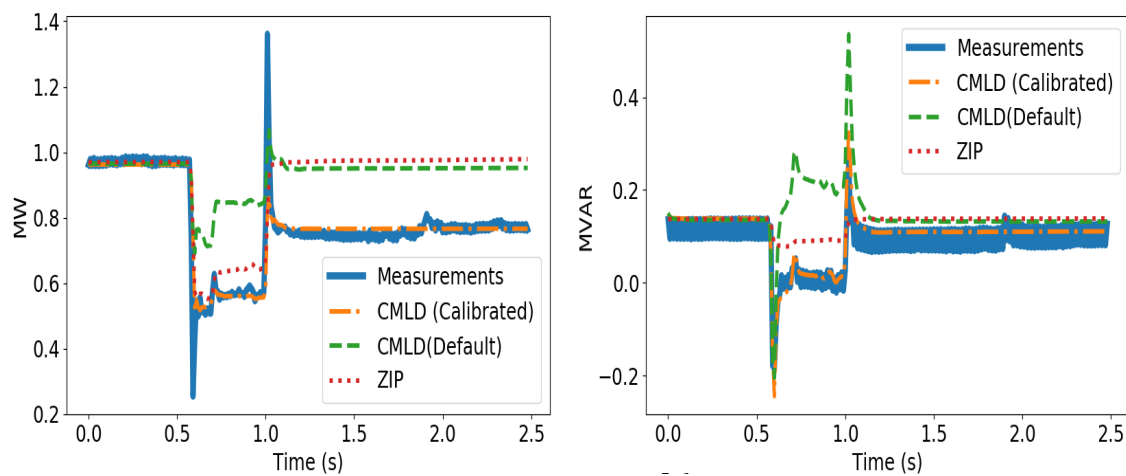


Figure 37: Estimation III: Active and reactive power outputs.

Table 26: Obtained parameters for additional experiments on various events.

Parameter	Event 1	Event 2	Event 3	Event 4
F_{mA}	0.109	0.000	0.000	0.001
F_{mB}	0.222	0.160	0.179	0.115
F_{mC}	0.000	0.000	0.000	0.000
F_{mD}	0.000	0.001	0.000	0.000
F_{el}	0.329	0.301	0.596	0.203
V_{d1}	0.840	0.840	0.787	0.355
V_{d2}	0.453	0.332	0.375	0.258
P_{Fs}	0.960	0.960	0.960	0.960
P_{1c}	0.515	0.580	0.150	0.600
P_{2c}	0.392	0.738	0.150	0.800
P_{frq}	1.692	1.049	0.901	0.727
Q_{1c}	1.800	1.784	1.784	1.265
Q_{2c}	1.500	1.500	1.071	1.497
Q_{frq}	-0.904	-0.805	-1.040	-0.862
F_{tr1}	0.208	0.417	0.050	0.076
V_{tr1}	0.657	0.716	0.733	0.695
F_{tr2}	0.364	0.343	0.272	0.584
F_{rcel}	0.834	0.621	0.866	0.719
$J(\mathbf{z}_0)$	7.199	8.78	33.85	1.007
$J(\mathbf{z}^*)$	1.622	0.980	2.660	0.258

3.3.5 Additional Experiments

In this section, we estimate the WECC-CMLD parameters using data of different disturbances in Australia. An identical approach to the one explained in Section 3.3.4 was conducted, where the lower and upper bounds as well as the default values of the parameters are given in Table 25. The solutions obtained by the SQP algorithm are summarized in Table 26. The four selected events are described as follows:

1. The first event occurred at Feeder Y on January 4, 2018 at 20:27:39. The output of the model with calibrated and default parameters is shown in Fig. 38. The obtained parameters are given in the second column of Table 26. After convergence, the objective function was reduced from 7.199 to 1.622.
2. The second event took place at Feeder Y on May 1, 2018 at 17:25:30. The output of the model with calibrated and default parameters is shown in Fig. 39. The obtained parameters are given in the third column of Table 26. After convergence, the objective function was reduced from 8.780 to 0.980.
3. The third event took place at Feeder Y on June 19, 2018 at 17:26:09. The output of the model with calibrated and default parameters is shown in Fig. 40. The values of the calibrated parameters are shown in the fourth column of Table 26. After convergence, the objective function was reduced from 33.850 to 2.660.
4. The fourth event took place at Feeder Y on July 31, 2018 at 22:51:24. The output of the model with default and calibrated parameters is shown in Fig. 41. The calibrated parameters are given

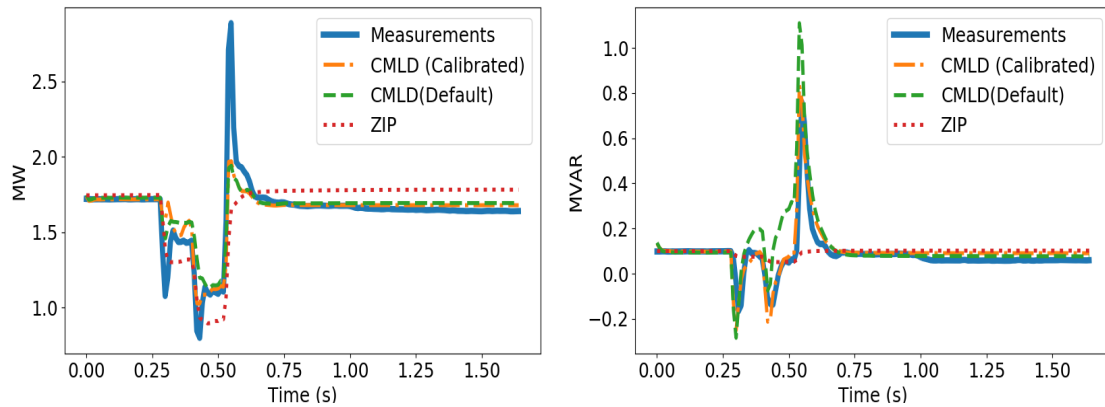


Figure 38: Event 1: Feeder Y, January 4 2018 at 20:27:39

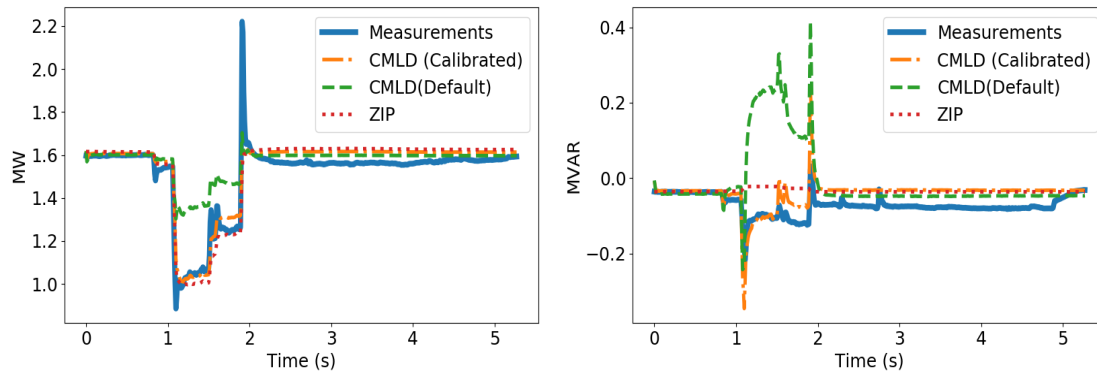


Figure 39: Event 2: Feeder Y, May 1, 2018 at 18:27:38

in the last column of Table 26. The objective function was reduced from 1.007 to 0.258.

As observed in Figs. 38, 39, 40 and 41, the calibrated WECC-CMLD outperforms the model with default parameters and the conventional ZIP model.

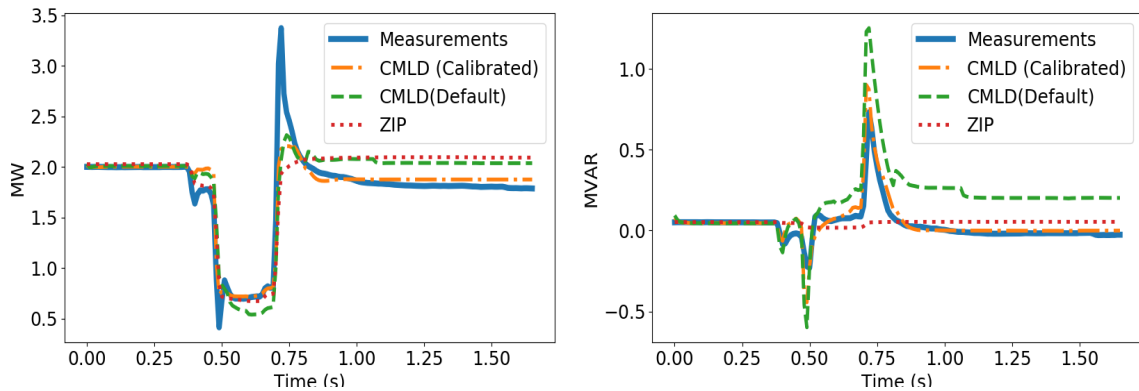


Figure 40: Event 3: Feeder Y, June 19 2017 at 17:25:38

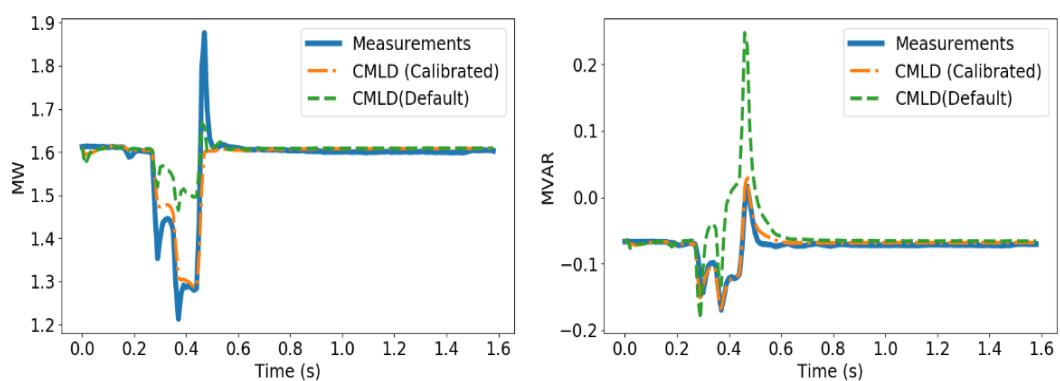


Figure 41: Event 4: Feeder Y, July 31, 2018 at 22:51:24

3.4 Future Work

3.4.1 WECC-CMLD Parameter Estimation

Our results indicate the hybrid component-based and measurement-based approach for estimating the parameters of the WECC-CMLD leads to a better emulation of aggregate behaviour of loads at different feeders in Australia. The component-based approach alone seems unable to accurately capture the dynamics of the load for different types of disturbances, it requires a measurement-based approach to calibrate its parameters according to the particular type of disturbance, time of the day, weather conditions and so on. The measurement-based approach, however, needs further improvements. Thus far, the WECC-CMLD parameters are calibrated separately for each disturbance. In the next few months, the measurement-based approach will be modified as to consider multiple disturbances simultaneously to calibrate the parameters of the WECC-CMLD. More specifically, if measurements from more than one disturbance are considered and the data of disturbance k are represented as $\hat{\mathbf{v}}_k(t)$, $\hat{P}_k(t)$ and $\hat{Q}_k(t)$, the objective function of the measurement-based approach will be modified as follows:

$$J(\mathbf{z}) = \sum_{k=0}^K \left(\int_{t_{k,0}}^{t_{k,f}} w_{k,p} (\hat{P}_k(t) - P_{cmld}(t, \mathbf{x}, \mathbf{z}, \mathbf{c}, \hat{\mathbf{v}}_k(t)))^2 dt + \int_{t_{k,0}}^{t_{k,f}} w_{k,q} (\hat{Q}_k(t) - Q_{cmld}(t, \mathbf{x}, \mathbf{z}, \mathbf{c}, \hat{\mathbf{v}}_k(t)))^2 dt \right), \quad (38)$$

The above problem requires further developments in the computational tool. It is also k times more computationally expensive than the current measurement-based approach.

3.4.2 Incorporation of DER Dynamics

The aggregate dynamics of DER represented by the DER_A model (presented in the Milestone1 report) will be added in the parameter calibration process. The new output considering the dynamics of DER_A will be derived and incorporated in the total active and reactive power output of the model in equations (35) and (36). In the next release of the parameter calibration tool, the parameters of DER_A will be included in the optimization algorithm.

4 CONCLUSIONS

Based on inverter bench testing results and the DER-load modelling work, we can highlight the following facts:

- We observe a wide variety of inverter behaviours. This fact complicates the development of a single aggregate model for all PV inverters. We believe that an aggregate model is possible for steady-state studies where all important variables—such as voltage amplitude and frequency—are changing slowly. For a single aggregate model, the change in voltage amplitude and frequency should be slow and resemble the AS4777 compliance tests.
- For rapid changes in voltage amplitude and frequency, also referred as sub-cycle threats, more than one model may be needed. For instance, one model for phase jumps and short-duration voltage sags and one model for high RoCoF during faults.
- The timescales at which inverters sample, process and make decisions may be 2-3 orders of magnitude faster than conventional power system equipment. It is imperative to consider this fact when developing a model for the sub-cycle threats explained above. This requires the use appropriate tools capable of time-steps smaller than $100\mu s$.
- Our attempts at understanding inverter behaviours based on grid incidents using combinations of high-frequency data, Solar Analytics data, and bench testing is improving but needs more time, ‘deeper’ inverter testing, and better visibility of the network (more measurement nodes and higher sample rates).
- We need to develop better models to simulate feeder systems. The high-frequency data measured at the primary (11kV) helps determine the phase jump, but other factors may be important, such as transformers and other power system equipment or control, in terms of the voltages seen at the inverter terminals.
- The composite load model parameter estimation approach needs further improvements. More than one contingency should be considered in the parameter calibration process and this requires changes in the current version of the tool.
- DERs dynamics should be added into the parameter calibration process. The current version only supports the composite load model parameters and the DER model should be added in future releases.
- The electrical parameters of induction motors A, B and C in the WECC-CMLD may help us to provide a better fit between the model output and the measured data. An attempt to calibrate these parameters should be conducted. This however requires the integration of additional constraints and bounds in the optimization problem.
- The DER_A model introduced in the Milestone 1 report should be modified in order to support different versions of the AS4777 standard. At the moment, two different models are being used to represent the two versions of the AS4777. However, future modifications in the standard should be easily adapted in the DER_A model.

References

- [1] D Kraft *A Software Package for Sequential Quadratic Programming* Forschungsbericht. Deutsche Forschungs- und Versuchsanstalt für Luft- und Raumfahrt, DFVLR, 1988
- [2] Qiuhua Huang and Renke Huang and Bruce J. Palmer and Yuan Liu and Shuangshuang Jin and Ruisheng Diao and Yousu Chen and Yu Zhang *A Reference Implementation of WECC Composite Load Model in Matlab and GridPACK*, <http://arxiv.org/abs/1708.00939>
- [3] *Grid Connection of Energy Systems via Inverters. Part 3: Grid Protection Requirements*, Standards Australia/Standards New Zealand Std. AS 4777.3, 2005.
- [4] *Grid Connection of Energy Systems via Inverters. Part 2: Inverter Requirements*, Standards Australia/Standards New Zealand Std. AS 4777.2, 2015.
- [5] *Distributed Energy Resources Connection with the Grid*, Technical Specification IEC TS 62786, International Electrotechnical Commission, April 2017.
- [6] M. T. Haque, *Single-phase PQ theory*, in Proc. 33rd Annu. IEEE Power Electronics Specialists Conference, Cairns, QLD, Australia, 2002, pp. 1815-1819, vol. 4.
- [7] *IEEE Standard for Interconnection and Interoperability of Distributed Energy Resources with Associated Electric Power Systems Interfaces*, in IEEE Std 1547-2018 (Revision of IEEE Std 1547-2003) pp.1-138, 6 April 2018
- [8] IEEE PES, *Technical Report PES-TR67: Impact of IEEE 1547 Standard on Smart Inverters*, May 2018, https://resourcecenter.ieee-pes.org/technical-publications/technical-reports/PES_TR0067_5-18.html.
- [9] M. H. Bollen, *Understanding Power Quality Problems: Voltage Sags and Interruptions*. Wiley, 2000.
- [10] *Generators connected to the low-voltage distribution network - Technical requirements for the connection to and parallel operation with low-voltage distribution networks*, English translation of VDE-AR-N 4105, Nov. 2018
- [11] Z. Y. Dong, A. Borghetti, K. Yamashita, A. Gaikwad, P. Pourbeik, J. V. Milanović *CIGRE WG C4.065 Recommendations on Measurement Based and Component Based Load Modelling Practice* in Fusion of Lightning Research and Practice for Power System in the Future; 10 Oct 2012-12 Oct 2012; Hakodate, Japan. 2012.
- [12] Anish Gaikwad, Penn Markham, Pouyan Pourbeik *Implementation of the WECC Composite Load Model for utilities using the component-based modeling approach* in IEEE TIEEE/PES Transmission and Distribution Conference and Exposition (T&D), May 2016
- [13] Jae-Kyeong Kim, Kyungsung An, Jin Ma, Jeonghoon Shin, Kyung-Bin Song, Jung-Do Park, Jung-Wook Park, Kyeon Hur *Fast and Reliable Estimation of Composite Load Model Parameters Using Analytical Similarity of Parameter Sensitivity* in IEEE Transactions on Power Systems, vol. 31, NO. 1, January 2016.
- [14] AEMO *Technical Integration of Distributed Energy Resources: Improving DER capabilities to benefit consumers and the power system*, <https://www.aemo.com.au-/media/Files/Electricity/NEM/DER/2019/Technical-Integration/Technical-Integration-of-DER-Report.pdf>, April 2019.

- [15] Western Electricity Coordinating Council *WECC Dynamic Composite Load Model (CMPLDW) Specifications* <https://www.wecc.biz/Reliability/WECC>
- [16] Q. Huang, R. Huang, B.J. Palmer, Y. Liu, S. Jin, R. Diao *A generic modelling and development approach for WECC composite load model* Electric Power System Research 172(2019) 1-10
- [17] Georgios Konstantinou, Leonardo Callegaro, John Fletcher, Nelson Avila *From inverter standard to inverter behaviour for small-scale distributed generation* Asia Pacific Conference for Integration of Distributed Energy Resources, Melbourne, 20-21 Aug. 2019.
- [18] www.cleanenergyregulator.gov.au, accessed July 2019.
- [19] pv-map.apvi.org.au/postcode, accessed July 2019.

Contact: John Fletcher

Email: john.fletcher@unsw.edu.au

END